

AD-A167 716

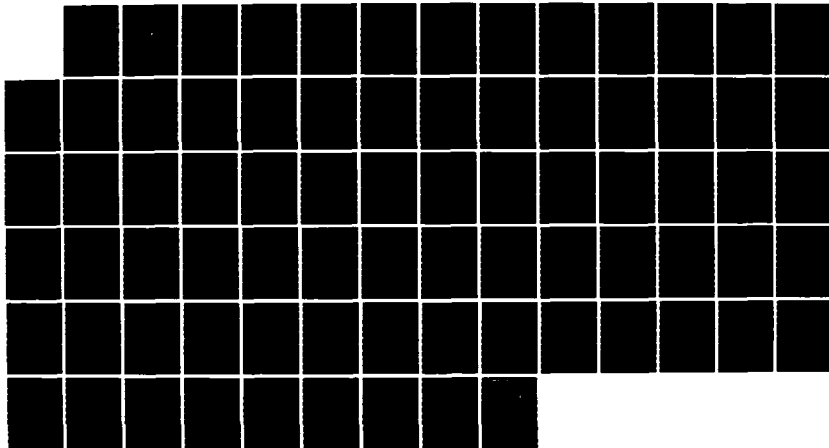
EFFECTS OF VARIABLE PROPERTIES IN FILM COOLED TURBULENT  
BOUNDARY LAYERS(U) NAVAL POSTGRADUATE SCHOOL MONTEREY  
CA A F HALZ MAR 86

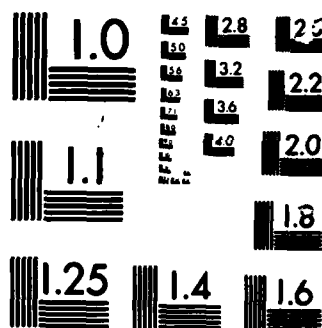
1/1

UNCLASSIFIED

F/G 20/4

NL





MICROCOPY

CHART

2

# NAVAL POSTGRADUATE SCHOOL

Monterey, California

AD-A167 716



DTIC  
ELECTE  
MAY 21 1986  
S E D

## THESIS

EFFECTS OF VARIABLE PROPERTIES  
IN FILM COOLED  
TURBULENT BOUNDARY LAYERS

by

Alfred Frank Walz Jr.

March 1986

Thesis Advisor:

P. M. Ligrani

Approved for public release; distribution unlimited

DTIC FILE COPY

REPRODUCED AT GOVERNMENT EXPENSE

UNCLASSIFIED

SECURITY CLASSIFICATION OF THIS PAGE

## REPORT DOCUMENTATION PAGE

1a REPORT SECURITY CLASSIFICATION <b>UNCLASSIFIED</b>			1b RESTRICTIVE MARKINGS	
2a SECURITY CLASSIFICATION AUTHORITY			3 DISTRIBUTION / AVAILABILITY OF REPORT  Approved for public release; distribution is unlimited	
2b DECLASSIFICATION / DOWNGRADING SCHEDULE				
4 PERFORMING ORGANIZATION REPORT NUMBER(S)			5 MONITORING ORGANIZATION REPORT NUMBER(S)	
6a NAME OF PERFORMING ORGANIZATION Naval Postgraduate School		6b OFFICE SYMBOL (If applicable) Code 69	7a NAME OF MONITORING ORGANIZATION Naval Postgraduate School	
6c ADDRESS (City, State, and ZIP Code) Monterey, California 93943-5000			7b ADDRESS (City, State, and ZIP Code) Monterey, California 93943-5000	
8a NAME OF FUNDING / SPONSORING ORGANIZATION		8b OFFICE SYMBOL (If applicable)	9 PROCUREMENT INSTRUMENT IDENTIFICATION NUMBER	
8c ADDRESS (City, State, and ZIP Code)			10 SOURCE OF FUNDING NUMBERS	
			PROGRAM ELEMENT NO	PROJECT NO
11 TITLE (Include Security Classification)  EFFECTS OF VARIABLE PROPERTIES IN FILM COOLED TURBULENT BOUNDARY LAYERS				
12 PERSONAL AUTHOR(S) Waltz, Alfred F., Jr.				
13a TYPE OF REPORT Master's Thesis		13b TIME COVERED FROM TO	14 DATE OF REPORT (Year, Month, Day) 1986 March	
15 PAGE COUNT 76				
16 SUPPLEMENTARY NOTATION  cont fr p 3				
17 COSATI CODES			18 SUBJECT TERMS (Continue on reverse if necessary and identify by block number)	
FIELD	GROUP	SUB-GROUP	Gas Turbine Cooling; Film Cooling; Turbulent Boundary Layers, Variable Properties, (Theor)	
19 ABSTRACT (Continue on reverse if necessary and identify by block number) The effects of variable properties on heat transfer in a film cooled turbulent boundary layer were investigated. A new procedure was developed to deduce adiabatic effectiveness from heat transfer coefficients based on the wall to freestream temperature difference, where both are representative of variable property flow conditions. The new technique was shown to be valid using data from the literature for injection into a turbulent boundary layer from one and two rows of injection holes. From these results, the variation of the coolant to mainstream density ratio was shown to have a significantly greater effect on heat transfer than variations of viscosity and thermal conductivity.				
20 DISTRIBUTION / AVAILABILITY OF ABSTRACT <input checked="" type="checkbox"/> UNCLASSIFIED/UNLIMITED <input type="checkbox"/> SAME AS RPT <input type="checkbox"/> DTIC USERS			21 ABSTRACT SECURITY CLASSIFICATION <b>UNCLASSIFIED</b>	
22a NAME OF RESPONSIBLE INDIVIDUAL P. M. Ligrani			22b TELEPHONE (Include Area Code) (408) 646-3382	22c OFFICE SYMBOL Code 69XX

Approved for public release; distribution is unlimited.

Effects of Variable Properties  
in Film Cooled  
Turbulent Boundary Layers

by

Alfred F. Walz Jr.  
Lieutenant Commander, United States Navy  
B.S., Maine Maritime Academy, 1977

Submitted in partial fulfillment of the  
requirements for the degree of

MASTER OF SCIENCE IN MECHANICAL ENGINEERING


from the

NAVAL POSTGRADUATE SCHOOL  
March 1986


Author:


  
Alfred F. Walz Jr.

Approved by:

  
R.M. Ligrani, Thesis Advisor

  
K.T. Yang, Second Reader

  
Paul J. Marto, Chairman,  
Department of Mechanical Engineering

  
John N. Dyer,  
Dean of Science and Engineering

# ABSTRACT

The effects of variable properties on heat transfer in a film-cooled turbulent boundary layer were investigated. A new procedure was developed to deduce adiabatic effectiveness from heat transfer coefficients based on the wall to freestream temperature difference, where both are representative of variable property flow conditions. The new technique was shown to be valid using data from the literature for injection into a turbulent boundary layer from one and two rows of injection holes. From these results, the variation of the coolant to mainstream density ratio was shown to have a significantly greater effect on heat transfer than variations of viscosity and thermal conductivity. Keywords: *→(p1)*

Accession For	
NTIS GRA&I	<input checked="" type="checkbox"/>
DTIC TAB	<input type="checkbox"/>
Unannounced	<input type="checkbox"/>
Justification	
By _____	
Distribution/ _____	
Availability Codes	
Dist	Avail and/or Special
A-1	



REPRODUCED AT GOVERNMENT EXPENSE

## TABLE OF CONTENTS

I.	INTRODUCTION . . . . .	10
II.	BACKGROUND . . . . .	11
	A. TURBINE BLADE COOLING FUNDMENTALS . . . . .	11
	B. FILM COOLING . . . . .	15
	C. BOUNDARY LAYER EQUATIONS . . . . .	16
III.	PRELIMINARY CONSIDERATIONS . . . . .	21
	A. CONSTANT PROPERTY CONSIDERATIONS . . . . .	21
	B. VARIABLE PROPERTY CONSIDERATIONS . . . . .	24
IV.	RESULTS . . . . .	27
	A. DATA OF PEDERSEN, ECKECT, AND GOLDSTEIN (1977) . . . . .	27
	B. DATA OF LIGRANI AND CAMCI (1985) . . . . .	28
V.	SUMMARY . . . . .	30
VI.	RECOMMENDATIONS . . . . .	31
	LIST OF REFERENCES . . . . .	32
	APPENDIX : FIGURES . . . . .	33
	INITIAL DISTRIBUTION LIST . . . . .	75

## LIST OF FIGURES

1.	The Development of the Turbine Entry Temperature . . . . .	33
2.	Methods of Turbine Blade Cooling . . . . .	34
3.	Characteristic Types of Blade Cooling Configurations . . . . .	35
4.	Coolant Flow in a Typical High Pressure Turbine Stage . . . . .	36
5.	Coolant Flow in a Typical Nozzle Guide Vane . . . . .	37
6.	Turbine Entry Temperature Verses Required Cooling Effectiveness . . . . .	38
7.	Comparative Cooling Requirements. Leading Edge Temperature 1000 C. Cooling Air Temperature 260 C . . . . .	39
8.	Film Cooling by a Row of Holes with Sample Temperature Profiles . . . . .	40
9.	Distribution of Heat Transfer Coefficient and Adiabatic Wall Temperature Around a Typical Blade . . . . .	41
10.	Curvilinear System of Coordinates . . . . .	42
11.	Viscosity and Thermal Conductivity of Common Gases at Low Pressures . . . . .	43
12.	Linear Variation of Heat Transfer Coefficient with Nondimensional Coolant Temperature . . . . .	44
13.	Domain Map of Blowing Ratio and Density Ratio for Pedersen, Eckert, and Goldstein (1977) Data . . . . .	45
14.	Nonlinear Variation of $h/h_0$ with $\theta$ . . . . .	46
15.	Effectiveness Verses $x/d$ from Pedersen, Eckert, and Goldstein (1977) . . . . .	47
16.	Variation of $\hat{h}/h_0$ with $\theta$ and $x/d$ for $M=0.213$ . . . . .	48
17.	Variation of $\hat{h}/h_0$ with $\theta$ and $x/d$ for $M=0.515$ . . . . .	49
18.	Variation of $\hat{h}/h_0$ with $\theta$ and $x/d$ for $M=1.05$ . . . . .	50
19.	Variation of $\hat{h}/h_0$ with $\theta$ and $x/d$ for $M=1.96$ . . . . .	51
20.	Variation of $h/h_0$ with $\theta$ for Two Rows of Injection from Ligriani and Camci (1985) . . . . .	52
21.	Variation of $\hat{n}$ with $x/d$ for $M=1.242$ . . . . .	53
22.	Variation of $\hat{n}$ with $x/d$ for $M=1.003$ . . . . .	54



23.	Variation of $\hat{n}$ with $x/d$ for $M=0.481$ . . . . .	55
24.	Variation of $\hat{n}$ with $x/d$ for $M=0.661$ . . . . .	56
25.	Variation of $\hat{n}$ with $x/d$ for $M=1.557$ . . . . .	57
26.	Variation of $\hat{n}$ with $x/d$ for $I=1.382$ . . . . .	58
27.	Variation of $\hat{n}$ with $x/d$ for $I=0.925$ . . . . .	59
28.	Variation of $\hat{n}$ with $x/d$ for $I=0.417$ . . . . .	60
29.	Variation of $\hat{n}$ with $x/d$ for $u_c/u_\infty=0.630$ . . . . .	61
30.	Variation of $\hat{n}$ with $x/d$ for $u_c/u_\infty=1.113$ . . . . .	62
31.	Variation of $\hat{n}$ with $x/d$ for $u_c/u_\infty=0.922$ . . . . .	63
32.	Variation of $\hat{n}$ with $\xi$ for $M=1.242$ . . . . .	64
33.	Variation of $\hat{n}$ with $\xi$ for $M=1.003$ . . . . .	65
34.	Variation of $\hat{n}$ with $\xi$ for $M=0.481$ . . . . .	66
35.	Variation of $\hat{n}$ with $\xi$ for $M=0.661$ . . . . .	67
36.	Variation of $\hat{n}$ with $\xi$ for $M=1.557$ . . . . .	68
37.	Variation of $\hat{n}$ with $\xi$ for $I=1.382$ . . . . .	69
38.	Variation of $\hat{n}$ with $\xi$ for $I=0.925$ . . . . .	70
39.	Variation of $\hat{n}$ with $\xi$ for $I=0.417$ . . . . .	71
40.	Variation of $\hat{n}$ with $\xi$ for $u_c/u_\infty=0.630$ . . . . .	72
41.	Variation of $\hat{n}$ with $\xi$ for $u_c/u_\infty=1.113$ . . . . .	73
42.	Variation of $\hat{n}$ with $\xi$ for $u_c/u_\infty=0.922$ . . . . .	74

## ACKNOWLEDGEMENTS

I would like to express my most sincere thanks to my loving wife, Julia Ann, and our children, James Robert and Travis Wayne, for their understanding and moral support while I attended the Naval Postgraduate School. Finally, I would like to thank Professor Phillip Ligrani for his help and patience while doing this thesis.

## NOMENCLATURE

- d - Injection Hole Diameter
- H - Enthalpy
- h - Heat Transfer Coefficient with Film Cooling  
(spanwise averaged),  $q''/(T_{O\infty} - T_w)$  and  $q''/(T_{r\infty} - T_w)$
- $h_f$  - Heat Transfer Coefficient with Film Cooling  
(spanwise averaged),  $q''/(T_{aw} - T_w)$
- $h_o$  - Heat Transfer Coefficient without Film Cooling  
(spanwise averaged),  $q''/(T_{O\infty} - T_w)$  and  $q''/(T_{r\infty} - T_w)$
- I - Injection Momentum Flux Ratio,  $\rho_c U_c^2 / \rho_\infty U_\infty^2$
- k - Thermal Conductivity
- m - Mole Fractions of Constitutant Gases
- M - Blowing Ratio,  $\rho_c U_c / \rho_\infty U_\infty$
- P - Static Pressure
- Pr - Molecular Prandtl Number
- $q''$  - Wall Heat Flux
- Re - Reynolds Number,  $\rho_c U_c d / \mu_c$
- T - Absolute Temperature
- U - Mean Velocity
- u - Velocity Component in X Direction
- v - Velocity Component in Y Direction
- W - Molecular Weights of Constitutant Gases
- x - Distance from Downstream Edge of Injection Holes

- $x/d$  - Nondimensional Distance
- $\alpha$  - Thermal Diffusivity
- $\rho$  - Density
- $\eta$  - Adiabatic Film Cooling Effectiveness (spanwise averaged), eqn. 15 and 22
- $\mu$  - Absolute Viscosity
- $\nu$  - Kinematic Viscosity
- $O$  - Nondimensional Coolant Temperature, eqn. 16
- $\gamma$  - Injection Angle Measured from Mainstream Flow Direction
- $\xi$  - Nondimensional Distance Parameter, eqn. 25
- $\lambda$  - Second Coefficient of Viscosity

#### SUBSCRIPTS

- aw - Adiabatic Wall
- c - Coolant
- e - Some Reference Value
- o - Total Condition
- r - Recovery Condition
- $\infty$  - Freestream

#### SUPERSCRIPTS

- $-$  - Averaged or Mean Value
- $\wedge$  - Variable Property
- $'$  - Fluctuation from the Averaged Value

## I. INTRODUCTION

Over the past thirty years, gas turbines have become smaller and lighter with improved fuel economy. These desirable characteristics have been achieved by raising the turbine entry temperatures. To prolong useful blade life in this high temperature environment, cooling systems, thermal barriers, and/or different materials capable of withstanding higher temperatures are utilized.

This thesis concentrates on film cooling. Film cooling protects components from high gas temperatures by blanketing the component with a film of cooler air. This film insulates the component and acts as a heat sink. The problem encountered with film cooling is the prediction of the component's wall temperature. Two different convective heat transfer coefficients are currently used for this prediction:

$$q'' = h_f(T_{aw} - T_w) \quad (1)$$

and

$$q'' = h(T_{o\infty} - T_w) \quad (2)$$

Here, different temperature differences are used to define  $h$  and  $h_f$ .

The objective of this thesis is to find a relation between the two heat transfer coefficients when the effects of variable properties are important.

## II. BACKGROUND

### A. TURBINE BLADE COOLING FUNDMENTALS

For a given size gas turbine, raising the turbine entry temperature results in a higher specific power. This enables the designer to operate the 'engine cycle' at a higher pressure ratio, resulting in improved thermal efficiency of the thermodynamic cycle and improved overall efficiency. The net result is a lower specific fuel consumption.

Raising the turbine entry temperature results in higher component temperatures. These components become more prone to failure at higher temperatures through greater oxidation rates of their surfaces, excessive creep, and/or by thermal fatigue. Figure 1 (Hennecke, 1982) shows a comparison of the rising turbine entry temperature to the rising blade material temperature limitations. Notice that uncooled metal components are limited to a turbine entry temperature of approximately 1200 K. Current fuel economy goals require a turbine entry temperature of 1600 K and greater. Numerous cooling systems have been devised to maintain internal components at or below their maximum allowable temperature. Vanes, blades, disks, liners, and casings may all require some form of cooling protection.

Figure 2 (Daniels and Schultz, 1982) illustrates two possible cooling medium schemes. Liquid systems use external sprays and/or internal convection methods. Air schemes use external films and/or internal convection methods. Liquid systems have several thermodynamic advantages over air systems. Despite these advantages, however, air systems have been universally accepted due to their relative mechanical simplicity to implement. Three principle methods of air cooling currently exist. They are

internal convection, film, and transpiration/effusion. Figure 3 (Hennecke, 1982) illustrates these characteristic types of cooling for turbine blades.

Internal convection is cooling by convection between the internal sections of the blade and the air. This type of cooling may be subdivided into several methods consisting of:

- (1) Straight through radial holes or channels of a single or multipass nature;
- (2) Enhanced heat transfer due to an enlargement of the internal surface area, promotion of turbulence, or impingement;
- (3) An insert that distributes the air according to the localized cooling requirements.

Film cooling is localized ejection of air through discrete slots or holes on the blade. This results in a film of air around the blade which is cooler than combustion gas temperature, acting as a heat sink. The film also acts like a thermal barrier between the hot gases and the blade's surface. This type of cooling may be subdivided into several methods consisting of:

- (1) Single films; where specific parts of the blade are covered by a film;
- (2) Full coverage; where many films are placed close enough together so they cover part or all of the blade.

Transpiration or effusion cooling is the bleeding of air through the blade at every point to form a protective film. The blade is made of a porous material to accomplish this method of cooling.

Typically, cooling air is extracted from various stages in the compressor and supplied to the components that require cooling. Figure 4 (Hennecke, 1982) illustrates the coolant flow path for a single stage of a typical gas turbine. Typical coolant flow rates as a percentage of the gas turbine's total flow rate are included. Notice that the guide vanes and turbine blades have the highest coolant flow rates. These two components are of primary concern for they

have the largest amount of surface area exposed to the mainstream flow and consequently the highest thermal loading.

Current applications use a combination of the internal convection and film cooling methods. Figure 5 (Daniels and Schultz, 1982) illustrates a typical guide vane cooling configuration. Cooling air comes in from the top and bottom of the vane. Notice the internal convection methods used:

- (1) Air is distributed to the internal surface;
- (2) Impingement on the surface after distribution;
- (3) Ribs and pedestals used to enlarge the surface area.

After the air has cooled the vane by internal convection, it is ejected into the mainstream and used as a film on the exterior surface. Initial stages utilize the internal convection and film cooling principles as illustrated in Figure 5. Latter stages may employ internal convection cooling solely due to the lower gas temperatures encountered in these stages.

The goal in using any cooling system is to maintain the internal components temperatures at or below their maximum allowable temperature. Achievement of this goal will result in high reliability and long service life. In addition, it is desirable to obtain (as closely as possible) a uniform blade temperature distribution to minimize thermal stresses.

In the selection of a cooling system to be employed, two key limitations must be kept in mind. These limitations are:

- (1) The minimal amount of cooling air should be used to minimize its detrimental effect on engine performance;
- (2) The effectiveness of a particular cooling method to keep the component sufficiently cooled for the desired turbine entry temperature.

The detrimental effect on engine performance is two fold. First, extracting air from the compressor reduces the available output power. Some work can be recovered by reintroducing the cooling air back into the mainstream flow



after cooling. Second, ejection of air through the blade has a detrimental effect on the aerodynamic efficiency of the turbine. Diminished aerodynamic efficiency results from pressure losses and flow separation in the wakes trailing the blades.

Figure 6 (Hennecke, 1982) shows the effectiveness of different methods used to cool components as a function of the turbine entry temperature. 'Cooling effectiveness' is defined as the ratio of actual to theoretical blade temperature reduction. This 'cooling effectiveness' is not only a function of the geometric configuration involved, but also the coolant flow rate. As the turbine entry temperature increases, so must the required cooling effectiveness.

Figure 7 shows the cooling flow required by various cooling methods as a function of the turbine entry temperature. Notice that convection cooling requires the most cooling flow rate while effusion requires the least at any given turbine entry temperature. Although this figure is for specific leading edge and coolant temperatures, the trend is the same for other temperature combinations.

Figures 6 and 7 indicate that to achieve the highest possible turbine entry temperature with minimum detrimental effects, effusion cooling should be used. Effusion cooling, however, is not currently used due to structural and manufacturing difficulties, and because the porous blades often become clogged. This is one reason why film cooling methods are currently employed.

Logically, one could assume that the more coolant pumped into the film and the fuller the coverage, the higher the turbine entry temperature. However, there are limitations:

- (1) The detrimental aerodynamic effects of film cooling may offset the gains of a higher turbine entry temperature;
- (2) "Lift-Off" may occur where the film ceases to protect the surface.

Thus, thermal design of vanes and blades with film cooling must be optimized.

## B. FILM COOLING

Film cooling is the ejection of coolant into the boundary layer on the blade. Figure 8 shows a typical film cooling geometry with temperature profiles for a row of holes. Notice on the top view, at some distance downstream, the flows from adjacent jets converge to form a continuous film over the blade's surface. In this region, lateral variations become negligible, allowing a two dimensional analysis to be conducted with reasonable accuracy.

The typical temperature profiles on Figure 8 illustrate the effect of film cooling on heat transfer. The left profile is without film cooling. Heat transfer is from the freestream to the blade's surface. The driving force is a function of the freestream recovery temperature and wall temperature. The right profile is with film cooling. Heat transfer is from the freestream to the coolant and from the coolant to the blade's surface. The driving force is a function of the freestream recovery temperature, coolant recovery temperature, and wall temperature. As the flow moves downstream from the injection site, the coolant mixes with the existing boundary layer. Eventually a temperature profile similar to the left will prevail. When this happens, the heat sink and insulating effects of the film become minimal.

Figure 9 illustrates a typical heat transfer coefficient and adiabatic wall temperature distribution around a turbine blade. Notice that the highest temperature and heat transfer coefficient occurs at the nose of the blade, near the stagnation point, and the location of the highest thermal loading. Because of this, injection sites are located in the nose and utilize the lowest coolant temperature. In the region around the stagnation point, the heat

transfer coefficients in Figure 9 are representative of a laminar boundary layer. At approximately one-fourth the distance along the suction surface, transition to a turbulent boundary layer begins, resulting in an increase in the adiabatic wall temperature and heat transfer coefficient approximately three-fourths the distance along the suction surface. The heat transfer coefficients along the pressure side in Figure 9 are representative of a turbulent boundary layer developing with a constant streamwise pressure gradient (after an initial drop from the stagnation point). Near the mid-chord position, the heat transfer coefficients begin to rise as a strong favorable pressure gradient develops.

### C. BOUNDARY LAYER EQUATIONS

To predict the heat flux from the mainstream to the blade, the equations governing the physical situation must be solved. Figure 10 illustrates the coordinate system used. Taking a differential element and applying the conservation principles of mass, momentum, and energy; the governing equations are derived. Using the governing equations, a solution to the heat transfer problem is considerably difficult since flow and temperature distributions are very complex. These equations are significantly simplified by making the following assumptions:

$$(1) \quad u \gg v$$

$$(2) \quad \frac{\partial P}{\partial y} \approx 0$$

$$(3) \quad \frac{\partial T}{\partial y} \gg \frac{\partial T}{\partial x}$$

$$(4) \quad \lambda + \frac{2}{3}\mu = 0$$

(5) No internal heat sources exist

(6) No chemical reactions occur within the element

(7) Body forces are negligible

(8) No work is performed by external fields

Applying these assumptions reduces the governing equations to the boundary layer equations. For turbulent boundary layers, the following form is for time-averaged velocities and variable properties:

### CONTINUITY

$$\frac{\partial}{\partial x}(\bar{\rho} \bar{u}) + \frac{\partial}{\partial y}(\bar{\rho} \bar{v}) = 0 \quad (3)$$

### MOMENTUM

$$(\bar{\rho} \bar{u}) \frac{\partial \bar{u}}{\partial x} + (\bar{\rho} \bar{v}) \frac{\partial \bar{u}}{\partial y} = - \frac{d\bar{P}}{dx} + \frac{\partial}{\partial y} \left( \mu \frac{\partial \bar{u}}{\partial y} - \overline{\rho u' v'} \right) \quad (4)$$

### ENERGY

$$(\bar{\rho} \bar{u}) \frac{\partial \bar{H}}{\partial x} + (\bar{\rho} \bar{v}) \frac{\partial \bar{H}}{\partial y} = \bar{u} \frac{d\bar{P}}{dx} + \frac{\partial q}{\partial y} + \tau \frac{\partial \bar{u}}{\partial y} \quad (5)$$

where

$$\tau = \mu \frac{\partial \bar{u}}{\partial y} - \overline{\rho u' v'} \quad (6)$$

and

$$q = k \frac{\partial \bar{T}}{\partial y} - \overline{\rho v' H'} \quad (7)$$

The boundary layer equations, as presented, are highly nonlinear. The momentum and energy equations are coupled through the temperature dependency of density and viscosity. Thermal conductivity is also temperature dependent. The

dependence of these transport properties on temperature results in different velocity/temperature profiles and different heat transfer coefficients from those obtained by assuming properties which are constant through the boundary layer.

Assuming constant properties exist through the boundary layer, the boundary layer equations may be rewritten as:

#### CONTINUITY

$$\frac{\partial \bar{u}}{\partial x} + \frac{\partial \bar{v}}{\partial y} = 0 \quad (8)$$

#### MOMENTUM

$$\bar{u} \frac{\partial \bar{u}}{\partial x} + \bar{v} \frac{\partial \bar{u}}{\partial y} = - \frac{1}{\rho} \frac{d\bar{P}}{dx} + \frac{\partial}{\partial y} \left( \mu \frac{\partial \bar{u}}{\partial y} - \overline{u'v'} \right) \quad (9)$$

#### ENERGY

$$\bar{u} \frac{\partial \bar{T}}{\partial x} + \bar{v} \frac{\partial \bar{T}}{\partial y} = \frac{\partial}{\partial y} \left( \alpha \frac{\partial \bar{T}}{\partial y} - \overline{v'T'} \right) \quad (10)$$

The momentum and energy equations ((9) and (10)) are uncoupled. This means that the momentum equation can be solved independently of the energy equation. In addition, the energy equation is linear. These two items simplify the process of solving the boundary layer equations.

A number of existing methods to account for variable properties in boundary layers without film cooling will now be discussed.

Mainstream gases consist of air and the combustion process by-products (principally Carbon Dioxide, Carbon Monoxide, and water vapor). Viscosity and thermal conductivity of this mixture can be determined though the semiempirical formula from White (1974):

$$\mu_{mix} = \frac{\sum_{i=1}^n m_i \mu_i}{\sum_{j=1}^n m_j \phi_{ij}} \quad (11)$$

where

$$\phi_{ij} = \frac{\{1 + (\mu_i/\mu_j)^{1/2} (W_j/W_i)^{1/4}\}^2}{(8 + 8W_i/W_j)^{1/2}} \quad (12)$$

This formula is for a mixture of  $n$  gases.  $W_i$  are the molecular weights and  $m_i$  are the mole fractions. The exact same formula is recommended for thermal conductivity ( $\mu$  is replaced by  $k$ ). Figure 11 (White (1974)) illustrates the temperature variations of viscosity and thermal conductivity for these gases at low pressures. Notice that for a 200 R temperature variation, the variations in viscosity and thermal conductivity are not very dramatic. A power law of the form (Kays and Crawford (1980)):

$$\frac{\mu_{mix}}{\mu_{mix_e}} = \frac{k_{mix}}{k_{mix_e}} = \left(\frac{T}{T_e}\right)^{0.68} \quad (13)$$

can be used to determine their temperature variations. For small temperature differences through boundary layers, say 20 C or less, viscosity and thermal conductivity may each be considered to be constant.

By considering the mainstream gases to be a perfect gas and from uniform static pressure through the boundary layer, the density variation becomes inversely proportional to the absolute temperature.

$$\frac{\rho}{\rho_e} = \frac{T_e}{T} \quad (14)$$

Comparsion of equations 13 and 14 shows that temperature variations result in larger density ratio changes than  $\mu$  or  $k$  changes.

### III. PRELIMINARY CONSIDERATIONS

The objectives in the thermal design of gas turbine blades are to obtain an acceptable stress level and design life. To do this, a detailed blade temperature distribution must be obtained.

The thermal design of a cooled turbine blade is a complicated energy balance. The design process can be broken down into three major categories outlined below (in sequential order):

- (1) Predicting the heat flux from the hot mainstream gases to the blade's surface;
- (2) Performing a conduction analysis for the detailed mapping of the blade's temperature distribution;
- (3) Predicting the heat flux from the blade to the internal cooling air.

This thesis only addresses the first category: a relation is developed and verified between the two types of heat transfer coefficient used to predict wall temperature.

#### A. CONSTANT PROPERTY CONSIDERATIONS

Equations 1 and 2 are used to calculate the blade's wall temperature after the heat flux is obtained by solving the boundary layer equations.

$$q'' = h_f(T_{aw} - T_w) \quad (1)$$

and

$$q'' = h(T_{o\infty} - T_w) \quad (2)$$

Both equations reflect the presence of film cooling.

In developing thermal boundary layers with film cooling, an adiabatic wall boundary condition can be used to describe the convection process. Using this concept reduces the driving potential from a three temperature potential problem



to a two temperature potential problem. Equation 1 represents this concept. Here,  $h_f$  is an isoenergetic heat transfer coefficient. The adiabatic wall temperature,  $T_{aw}$ , is the wall temperature when there is no heat transfer to the wall. Adiabatic wall temperature is usually expressed nondimensionally in terms of the adiabatic film cooling effectiveness,  $\eta$ :

$$\eta = \frac{T_{aw} - T_{r\infty}}{T_{rc} - T_{r\infty}} \quad (15)$$

Since the entire surface is considered adiabatic,  $T_{aw}$  is a global parameter. As a result, equation 1 is dependent on the entire convection process and the thermal boundary layer.

Compared to the large temperature differences between the mainstream gases and the blade's surface, the surface temperature distribution can be considered relatively isothermal. An isothermal wall is ideal since thermal stresses are minimal. Equation 2 represents this concept. Here,  $\theta$  is defined by the freestream stagnation temperature and the wall temperature difference for a specific coolant temperature. The coolant temperature is usually expressed nondimensionally as  $\theta$ :

$$\theta = \frac{T_{rc} - T_{r\infty}}{T_w - T_{r\infty}} \quad (16)$$

There has been considerable controversy over these two methods of predicting the wall's temperature. Two key issues of this controversy deal with how the temperature difference is defined and the effects of changing coolant parameters (temperature, density, mass flow rate, etc.). In equation 1, when the temperature difference equals zero, there is no heat transfer. This is not necessarily true if

equation 2 is used. To account for viscous dissipation, the freestream stagnation temperature,  $T_{0\infty}$ , is replaced by the freestream recovery temperature,  $T_{r\infty}$ . The heat transfer coefficient,  $h$ , is then redefined as:

$$q'' = h(T_{r\infty} - T_w) \quad (17)$$

Changing the film cooling parameters will have different effects on these equations. Generally, the recovery temperature is determined from freestream conditions (temperature, velocity, density), however, if it is based on near wall conditions, the recovery temperature in a film cooled boundary layer is the same as the adiabatic wall temperature. In equation 1, both  $h_f$  and  $T_{aw}$  are affected, whereas, in equation 17 only  $h$  is affected.

For a given location, the heat flux will be the same for either method. As such, equation 1 is set equal to equation 17 and a relation between the heat transfer coefficients exists. Using the definitions of  $\eta$  and  $\theta$ , and dividing by the heat transfer coefficient for the case of no film cooling, then yields:

$$\frac{h}{h_o} = \frac{h_f}{h_o}(1 - \eta\theta) \quad (18)$$

This equation relates adiabatic and isothermal wall boundary conditions for properties that are constant through the film cooled boundary layer. This relationship is plotted on Figure 12 (Ville, Cunat, and Richards, 1978). Note the linearity between  $h/h_o$  and  $\theta$ . This linearity is due to the fact that the energy equation is linear for constant properties. This equation is valid for a given downstream location, where adiabatic conditions are represented by the horizontal intercept, and isothermal conditions by the line.

On Figure 12, the axis intercept points have special meaning. The  $h/h_0$  axis intercept point represents the heat transfer coefficient when the coolant is injected at the same temperature as the mainstream ( $T_{rc}=T_{r\infty}$ ,  $\theta=0$ ). The  $\theta$  axis intercept point indicates a wall condition that is locally adiabatic. At this point,  $\theta$  equals the inverse of the effectiveness,  $\eta$ .

Figure 12 is only good for one downstream location. As you move further downstream, the slope of the curve becomes less and may eventually become horizontal indicating no cooling effect from the film. This is a result of a rising film temperature due to heat transfer, diffusion, and mixing with mainstream gases. As the film temperature rises, the value of  $\theta$  decreases and the value of  $\eta$  increases.

#### B. VARIABLE PROPERTY CONSIDERATIONS

With variable properties, the momentum and energy boundary layer equations become coupled because of the density term. In addition, the energy equation becomes highly nonlinear. Because of this, the linearity exhibited on Figure 12 no longer exists. Ligrani and Camci (1985) illustrated this nonlinearity that exists between  $h/h_0$  and  $\theta$ . They also derived an empirical relation to relate the constant property data of Jabbari and Goldstein (1978) to their variable property data.

To find the relation between  $\hat{h}/h_0$  and  $\theta$  for the variable property case, we start with the defining equations for the heat transfer coefficients.

For variable properties through the boundary layer, the variable property isoenergetic heat transfer coefficient,  $\hat{h}_f$ , is defined using:

$$q'' = \hat{h}_f(\hat{T}_{aw} - T_w) \quad (19)$$

The heat transfer coefficient,  $\hat{h}$ , is then defined using:

$$q'' = \hat{h}(T_{r\infty} - T_w) \quad (20)$$

The heat flux is now obtained by solving the variable property boundary layer equations. At a given location, the heat flux from equations 19 and 20 will be the same. Equating these gives:

$$\hat{h}_f(\hat{T}_{aw} - T_w) = \hat{h}(T_{r\infty} - T_w) \quad (21)$$

Now the adiabatic wall temperature is expressed in terms of an adiabatic film cooling effectiveness defined as:

$$\hat{\eta} = \frac{\hat{T}_{aw} - T_{r\infty}}{T_{rc} - T_{r\infty}} \quad (22)$$

$\theta$  is defined as before (equation 16). By substitution and rearrangement the variable property relation between  $\hat{h}/h_o$  and  $\theta$  then becomes:

$$\frac{\hat{h}}{h_o} = \frac{\hat{h}_f}{h_o}(1 - \hat{\eta}\theta) \quad (23)$$

This equation is for one downstream location at one value of the density ratio,  $\rho_c/\rho_\infty$ , and one value of any of the following; blowing ratio,  $M$ ; momentum flux ratio,  $I$ ; or the velocity ratio,  $u_c/u_\infty$ . A different line results from equation 23 for each value of the effectiveness,  $\hat{\eta}$ , and the normalized heat transfer coefficient,  $\hat{h}_f/h_o$ . The effectiveness,  $\hat{\eta}$ , may have a strong dependence on the density ratio,  $\rho_c/\rho_\infty$ , as indicated by the single row film cooling data of Pedersen, Eckert, and Goldstein (1977).

Figure 13 is a domain map showing density ratio verses blowing ratio of the Pedersen, Eckert, and Goldstein (1977) data. The box symbols indicate that effectiveness has little or no dependence on the density ratio for low blowing ratios. The circle symbols indicate that effectiveness has a strong dependence on the density ratio. The triangles indicate that the effect of the density ratio on the effectiveness and heat transfer is highly nonlinear.

Figure 14 shows one possible effect of variable properties on  $\hat{h}/h_0$  verses  $\theta$  data. Here, each of the three linear curves represents equation 23 with a different  $\hat{\eta}$ . The same  $h_f/h_0$  was used for each line to simplify Figure 14. Now, each line is also for one value of the density ratio,  $\rho_c/\rho_\infty$ , which is equivalent to  $T_\infty/T_c$ . The variation of the density ratio with  $\theta$  is then given by:

$$\frac{\rho_\infty/\rho_c - 1}{T_w/T_{r\infty} - 1} = \theta \quad (24)$$

if  $T_c/T_\infty = T_{rc}/T_{r\infty}$  for constant  $T_w$ . The  $\theta$  for a given density ratio will then be a straight vertical line emanating from the horizontal axis. The intersection of this vertical line and equation 23 will be where a given  $\hat{h}/h_0$  data point is located. The curved line represents the collection of the  $\hat{h}/h_0$  verses  $\theta$  data points. It curves downward because of the way the data collects. As the density ratio increases (vertical lines move to the right), the effectiveness increases. This causes the  $\theta$  axis intercept point ( $1/\hat{\eta}$ ) to move to the left.

#### IV. RESULTS

Using equation 23, the adiabatic effectiveness was used to deduce  $\hat{h}/h_0$  using the data of Pedersen, Eckert, and Goldstein (1977) for one row of injection holes. In addition, the adiabatic effectiveness was deduced from  $\hat{h}/h_0$  and  $\hat{h}_f/h_0$  from the data of Ligrani and Camci (1985) for two rows of injection holes.

In the following sections, the results are presented.

##### A. DATA OF PEDERSEN, ECKERT, AND GOLDSTEIN (1977)

Figure 15 shows the Pedersen, Eckert, and Goldstein (1977) data used to deduce  $\hat{h}/h_0$ . Figure 13 gives the blowing ratio and the density ratio values for which  $\hat{\eta}$  was selected for deducing  $\hat{h}/h_0$ .

A value of 1.0 was assumed for the  $\hat{h}/h_0$  axis intercept. Although in many cases, a reasonable assumption, Metzger, Carper, and Swank (1968) showed that this axis intercept may not be equal to 1.0. They showed that the injection has an effect on the heat transfer coefficient even when the coolant is injected at the freestream temperature, primarily due to boundary layer thickening.

Normalized heat transfer coefficients as a function of  $\theta$  are shown on Figures 16 thru 19 for the Pedersen, Eckert, and Goldstein (1977) data. Four axes are used to denote four downstream locations ( $x/d$ ). The light linear lines represent equation 23 for a different value of effectiveness,  $\hat{\eta}$ . The dark lines represent the collection of  $\hat{h}/h_0$  verses  $\theta$  data points.

Figure 16 is for a blowing ratio,  $M$ , of 0.213. This figure shows that  $\hat{h}/h_0$  verses  $\theta$  is steeper at small  $x/d$  and becomes flatter as the distance from the injection site increases (increasing  $x/d$ ). This figure shows reasonable linearity with some nonlinearity near the injection site.

Figure 17 is for a blowing ratio,  $M$ , of 0.515. This figure shows the same trends as with Figure 16. Only now, the nonlinearity near the injection site is more pronounced and is also evident at a location further downstream.

Figure 18 is for a blowing ratio,  $M$ , of 1.05. This figure shows that the variation of  $\hat{h}/h_0$  with  $\theta$  is nonlinear. As the distance from the injection site increases (increasing  $x/d$ ), the  $\hat{h}/h_0$  variation with  $\theta$  becomes more horizontal. Notice that, in general, at a particular blowing ratio, the slope becomes more negative as  $\theta$  increases.

Figure 19 is for a blowing ratio,  $M$ , of 1.96. This figure shows a highly nonlinear behavior due to the 'lift-off' of film cooling jets from the wall, and possible penetration through the boundary layer.

#### B. DATA OF LIGRANI AND CAMCI (1985)

Figure 20 (Ligrani and Camci, 1985) illustrates the downward sloping trend for variable property  $\hat{h}/h_0$  verses  $\theta$  data. This figure also shows the linear  $h/h_0$  verses  $\theta$  data (constant property case). Notice the similarity between the variable property trend here and the trends of the Pedersen, Eckert, and Goldstein (1977) data on Figure 18.

Using  $\hat{h}/h_0$  and  $\hat{h}_f/h_0$  from Ligrani and Camci (1985),  $\hat{n}$  was deduced from equation 23. Results are plotted as a function of  $x/d$  in Figures 21 thru 31, and as a function of  $\xi$  in Figures 32 thru 42. The latter function,  $\xi$ , is a downstream distance normalized by the blowing ratio. It is defined by:

$$\xi = \frac{x + 1.909d}{MS} \left( Re_c \left( \frac{u_c}{u_\infty} \right) \right)^{-0.25} \quad (25)$$

where  $S=\pi d/6$  is the width of an equivalent two dimensional slot (Jabbari and Goldstein, 1978). Goldstein (1971) gives

two equations to predict laterally averaged effectiveness,  $\hat{\eta}$ , for two dimensional film cooling. These predictions are given by:

$$\bar{\eta} = (1 + 0.249\xi)^{-0.8} \quad (26)$$

and

$$\bar{\eta} = \frac{1.9\text{Pr}^{2/3}}{1 + 0.329\xi^{0.8}\beta} \quad (27)$$

where

$$\beta = 1 + 1.5(10^{-4})(\text{Re}_c \frac{\mu_c}{\mu_\infty}) \sin\gamma \quad (28)$$

These predictions are plotted on the  $\hat{\eta}$  verses  $\xi$  graphs (Figures 32 thru 42).

Figures 21 thru 42 are for different blowing ratios ( $M = 1.242, 1.003, 0.481, 0.661, 1.557$ ), momentum flux ratios ( $I = 1.382, 0.925, 0.417$ ), and velocity ratios ( $u_c/u_\infty = 0.630, 1.113, 0.922$ ). In general, these figures show that as the blowing ratio, momentum flux ratio, and velocity ratio increase, the adiabatic film cooling effectiveness increases. The largest increase in  $\hat{\eta}$  occurs for the highest value of  $O$ . This corresponds to the case of the highest density ration. On Figures 21 thru 31, the crossover point between the  $O1$  and  $O2$  curves moves downstream (from  $x/d = 20$  to  $x/d = 40$ ) as the momentum flux ratio and velocity ratio increase. On Figures 32 thru 42, as the blowing ratio, momentum flux ratio, and the velocity ratio decrease, the data moves to a higher value and spreads out. All data points on the  $\hat{\eta}$  verses  $\xi$  graphs are below the predictions of equations 26 and 27 but do follow the same trend as the predictions.



## V. SUMMARY

A relation was derived that relates the normalized heat transfer coefficients  $\hat{h}$  and  $\hat{h}_f$ . These heat transfer coefficients are for isothermal wall boundary conditions,  $\hat{h}$ , and adiabatic wall boundary conditions,  $\hat{h}_f$ . Each are for when variable properties are considered to exist through the boundary layer. This relation was presented as:

$$\frac{\hat{h}}{h_0} = \frac{\hat{h}_f}{h_0} (1 - \hat{\eta}\theta) \quad (25)$$

When the effects of variable properties are important in film cooled turbulent boundary layers, the variable property effectiveness,  $\hat{\eta}$ , and the above equation are valid for one density ratio and blowing ratio only.

The normalized heat transfer coefficient,  $\hat{h}/h_0$ , was deduced from the Pedersen, Eckert, and Goldstein (1977) data on injection with one row of holes. The adiabatic film cooling effectiveness,  $\hat{\eta}$ , was deduced from the Ligrani and Camci (1985) data on injection with two rows of holes. The data deduced from equation 23 showed the nonlinear trend of  $\hat{h}/h_0$  verses  $\theta$  and as the density ratio,  $\rho_c/\rho_\infty$ , varied.

The effect of density ratio on  $\hat{h}/h_0$  verses  $\theta$  results in a change of the characteristic curve from linear to nonlinear. This change is not always evident. It's existence or extent is dependent upon the injection parameters (blowing ratio, momentum flux ratio, and velocity ratio) and the downstream distance. This effect is due to the nonlinearity introduced into the energy equation and the coupling of the momentum and energy equations when variable properties through the boundary layer are considered.

## VI. RECOMMENDATIONS

Experiments need to be conducted to determine the accuracy and dependability of the proposed variable property relation on injection system geometry, injection flow rate parameters, fluid mechanics of the flow, the thermal boundary layer conditions, and other parameters. In order to completely verify the proposed equation, simultaneous measurements of variable property effectiveness and variable property heat transfer coefficients (based on the wall and recovery freestream temperature difference) need to be conducted.

# LIST OF REFERENCES

Daniels, L. C. and Schultz, D. L., "Heat Transfer Rate to Blade Profiles-Theory and Measurement in Transient Facilities", Film Cooling and Turbine Blade Heat Transfer, VKI LS 1982-02, von Karman Institute for Fluid Dynamics, Rhode-St-Genese, Feb. 22-26, 1982.

Goldstein, R. J., "Film Cooling", Advances in Heat Transfer, Vol. 7, Academic Press, New York and London, 1971, pp. 321.

Hennecke, D. K., "Turbine Blade Cooling in Aeroengines", Film Cooling and Turbine Blade Heat Transfer, VKI LS 1982-02, von Karman Institute for Fluid Dynamics, Rhode-St-Genese, Feb. 22-26, 1982.

Jabbari, M. Y. and Goldstein, R. J., "Adiabatic Wall Temperature and Heat Transfer Downstream of Injection Through Two Rows of Holes", Journal of Engineering for Power, Vol. 100, Apr. 1978, pp. 303-307.

Kays, W. M. and Crawford, M. E., Convective Heat and Mass Transfer, 2d ed., McGraw-Hill, New York, 1980.

Ligrani, P. M. and Camci, C., "Adiabatic Film Cooling Effectiveness from Heat Transfer Measurements in Compressible, Variable Property Flow", Journal of Heat Transfer, Vol. 107, May 1985, pp. 313-320.

Metzger, D. E., Carper, H. J., and Swank, L. R., "Heat Transfer with Film Cooling Near Nontangential Injection Slots", Journal of Engineering for Power, Apr. 1968, pp. 157-153.

Pedersen, D. R., Eckert, E. R. G., and Goldstein, R. J., "Film Cooling With Large Density Differences Between the Mainstream and the Secondary Fluid Measured by the Heat Transfer Analogy", Journal of Heat Transfer, Vol. 99, Nov. 1977, pp. 620-627.

Ville, J-P., Cunat, D., and Richards, B. E., "The Measurement of Film Cooling Effectiveness in Short Duration Wind Tunnels", VKI Technical Note 127, von Karman Institute for Fluid Dynamics, Rhode-St-Genese, Dec. 1978.

White, F. M., Viscous Fluid Flow, McGraw-Hill, New York, 1974.

APPENDIX  
FIGURES

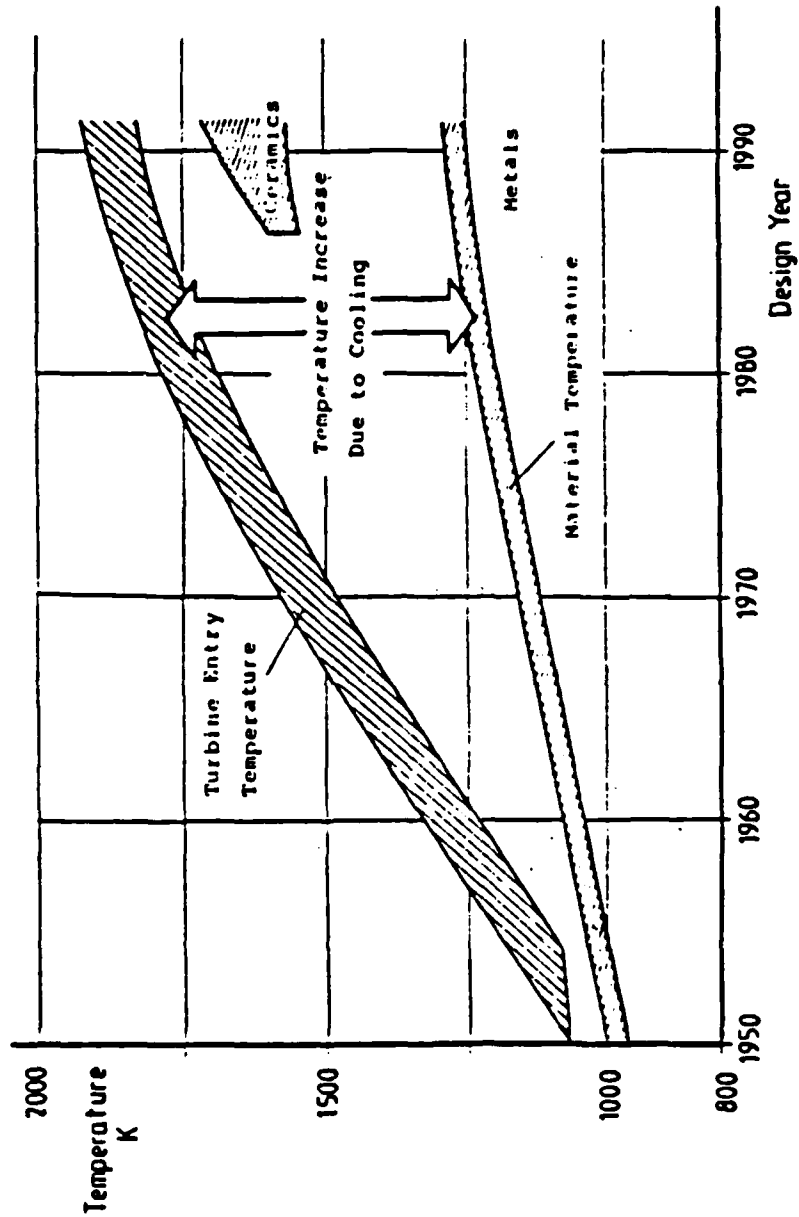


Fig. 1 The Development of the Turbine Entry Temperature.

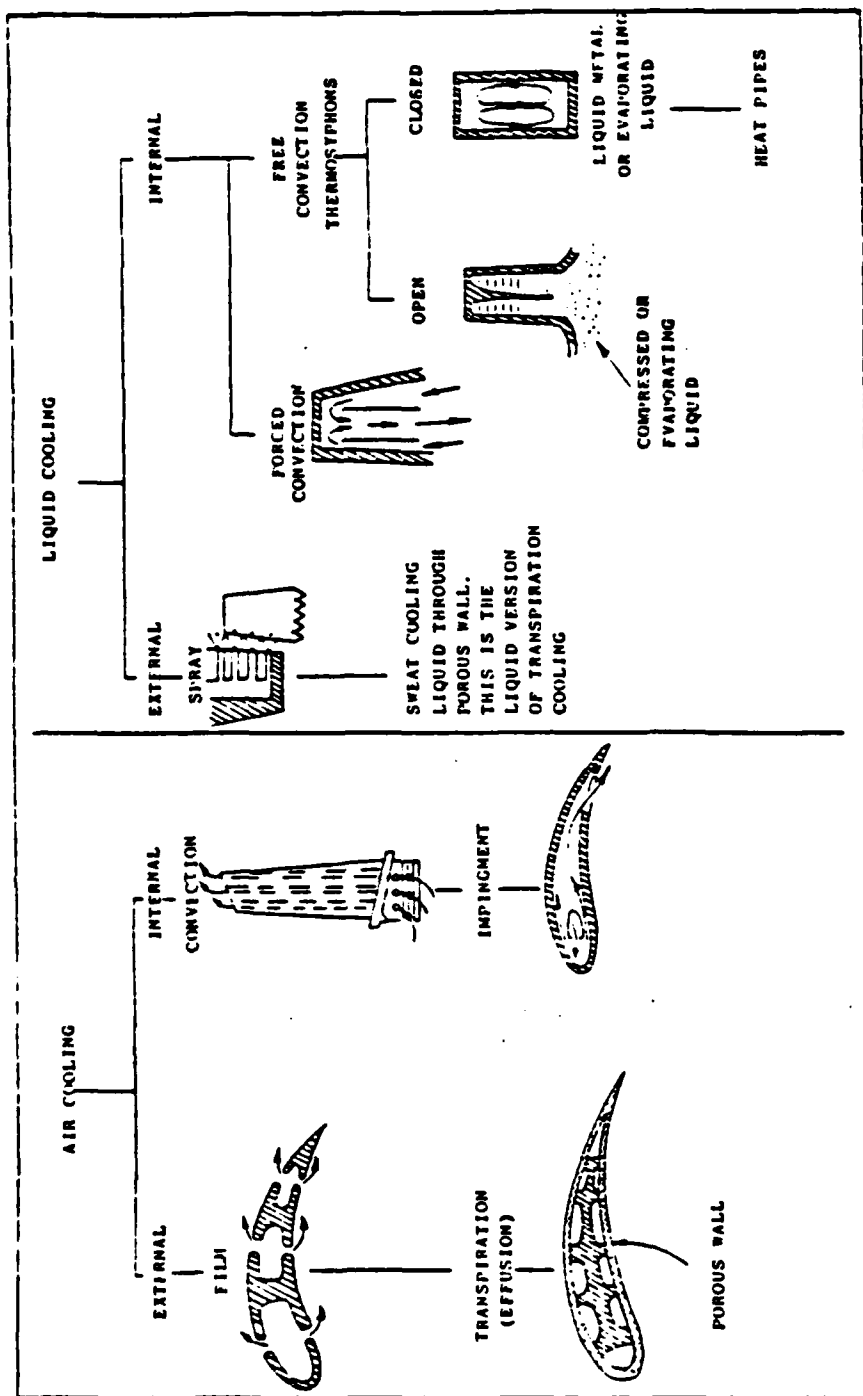
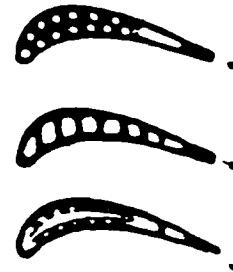


Fig. 2 Methods of Turbine Blade Cooling.

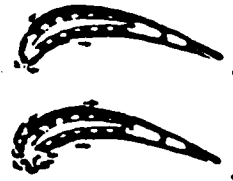
### 1. Internal Cooling

- straight through  
or multipass
- enhanced heat transfer
- insert



### 2. Film Cooling

- single films
- full coverage



### 3. Effusion Cooling



Fig. 3 Characteristic Types of Blade Cooling Configurations.

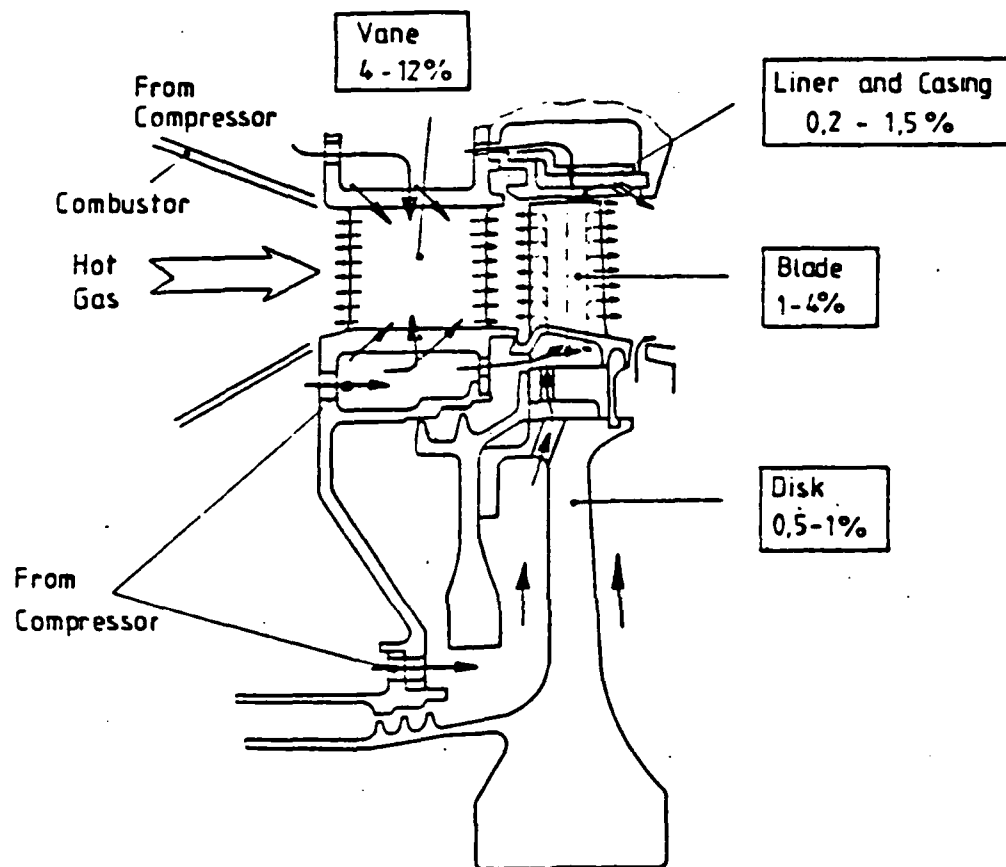


Fig. 4 Coolant Flow in a Typical High Pressure Turbine Stage.

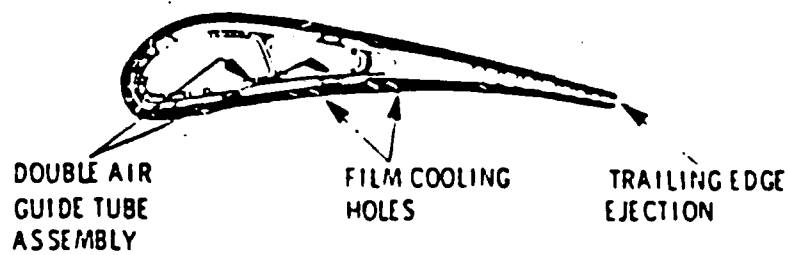
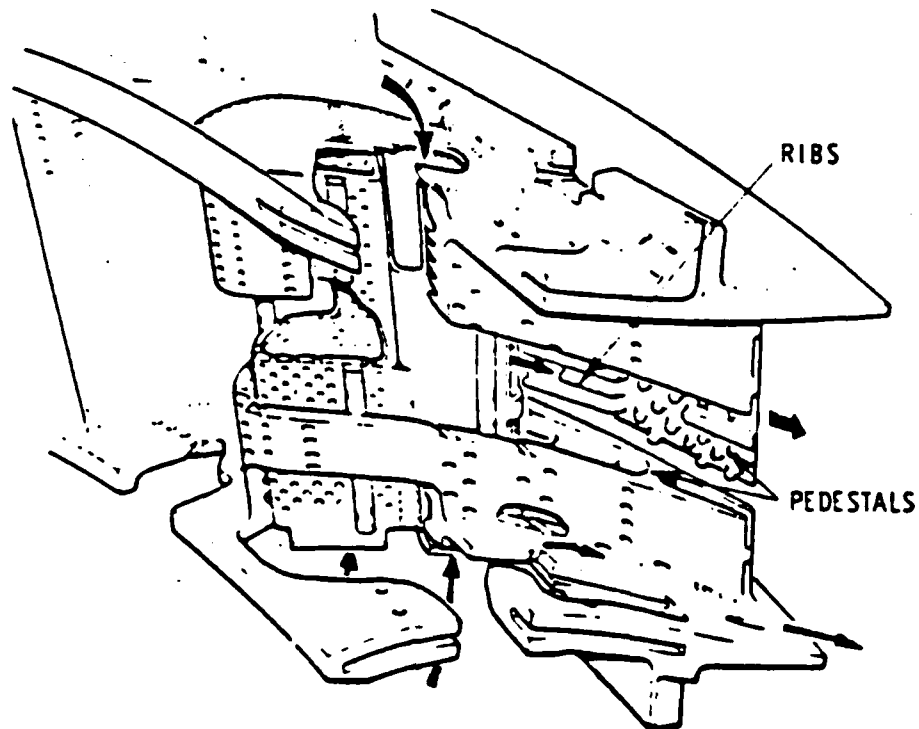


Fig. 5 Coolant Flow in a Typical  
Nozzle Guide Vane.



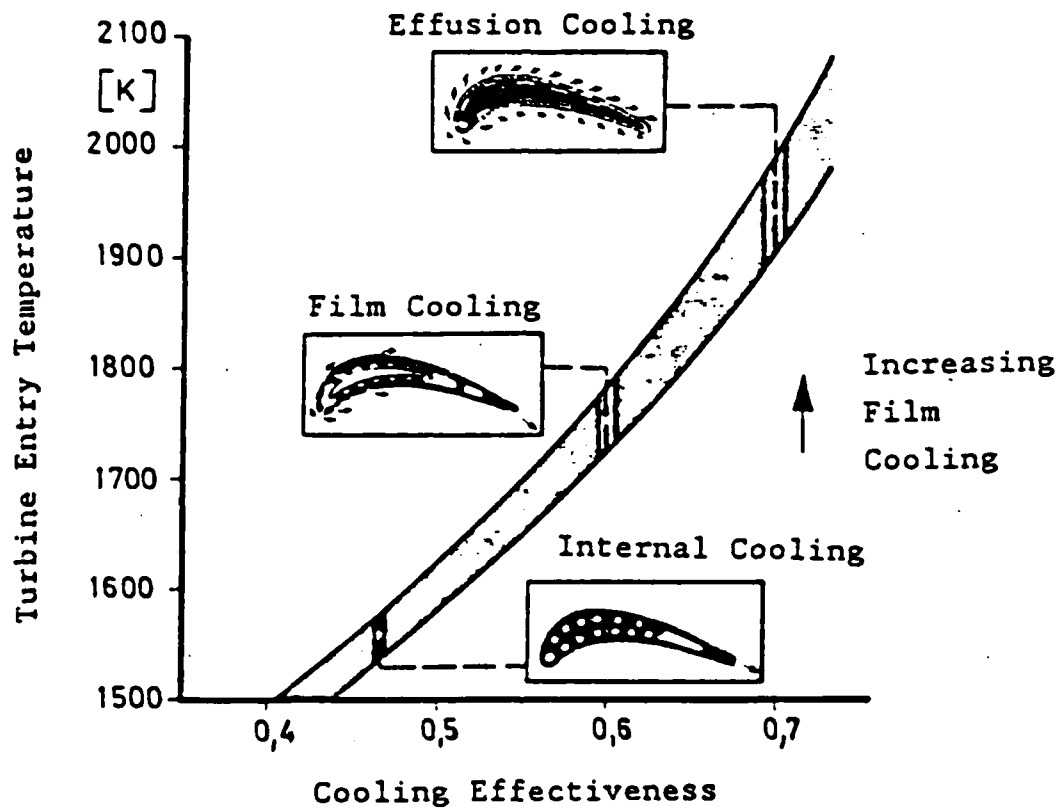


Fig. 6 Turbine Entry Temperature Verses Required Cooling Effectiveness.

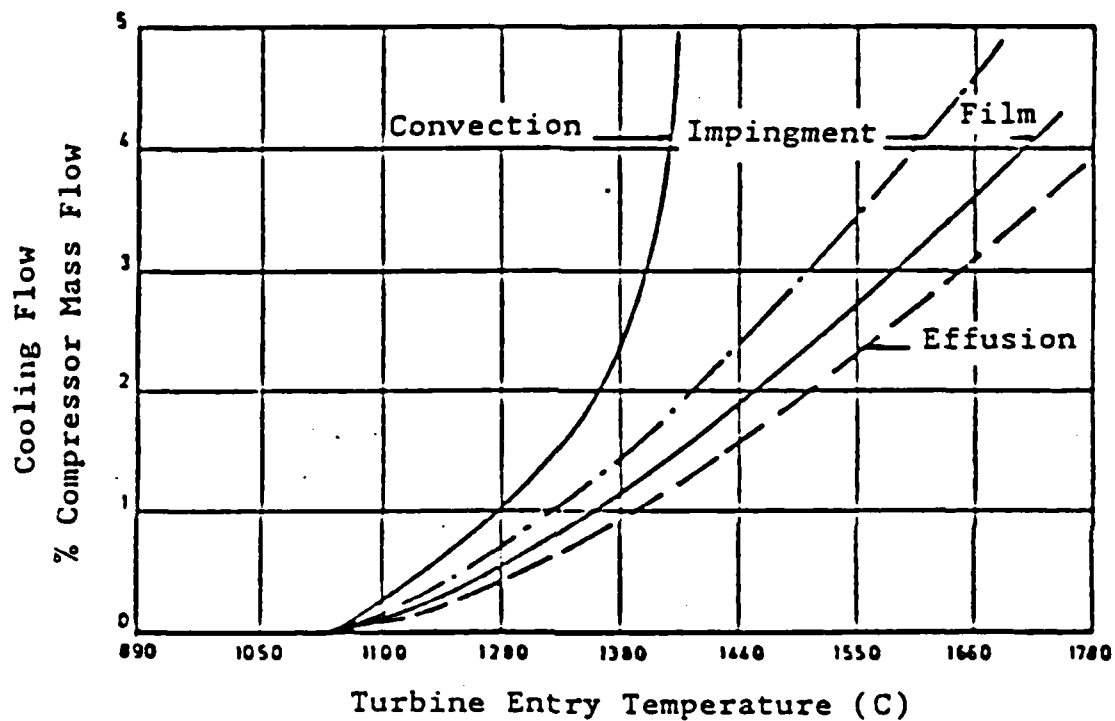
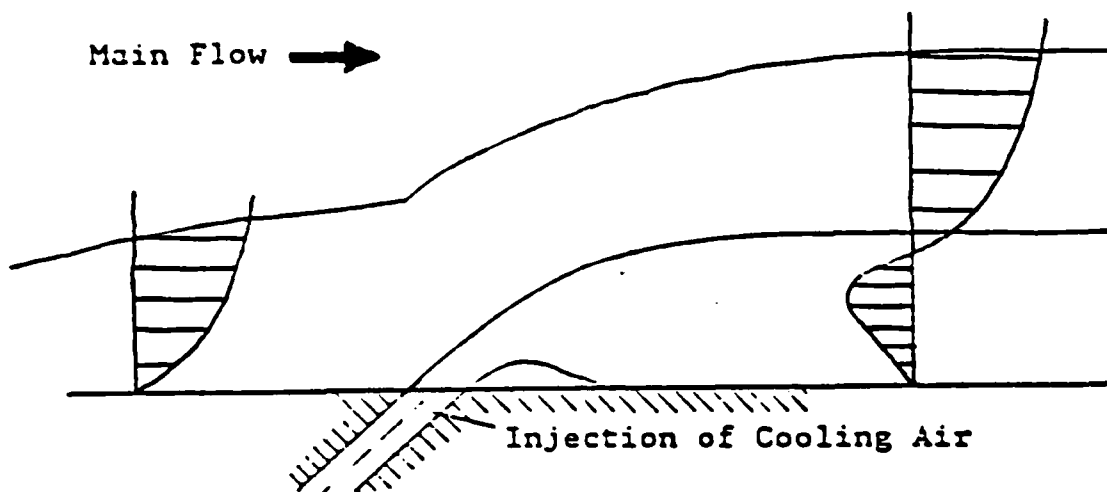


Fig. 7 Comparative Cooling Requirements.  
Leading Edge Temperature 1000 C.  
Cooling Air Temperature 260 C.



Region of Single Jets

Mixed Region

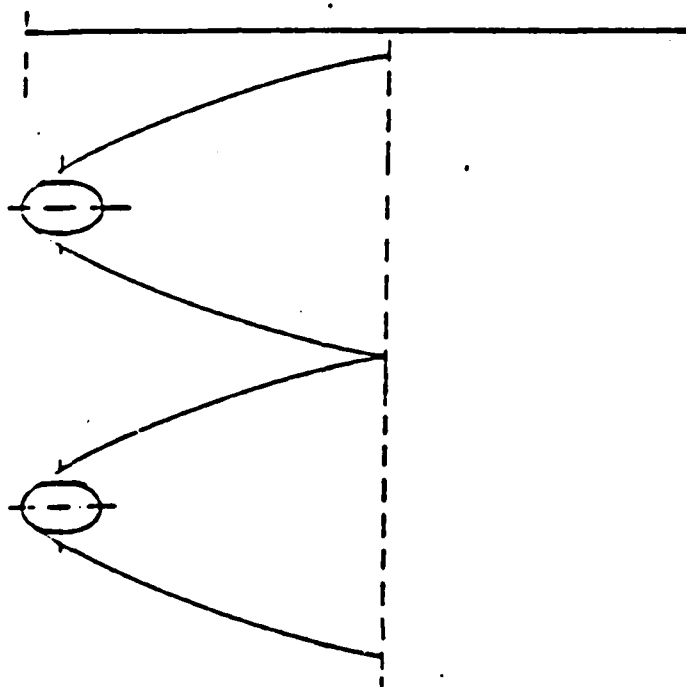
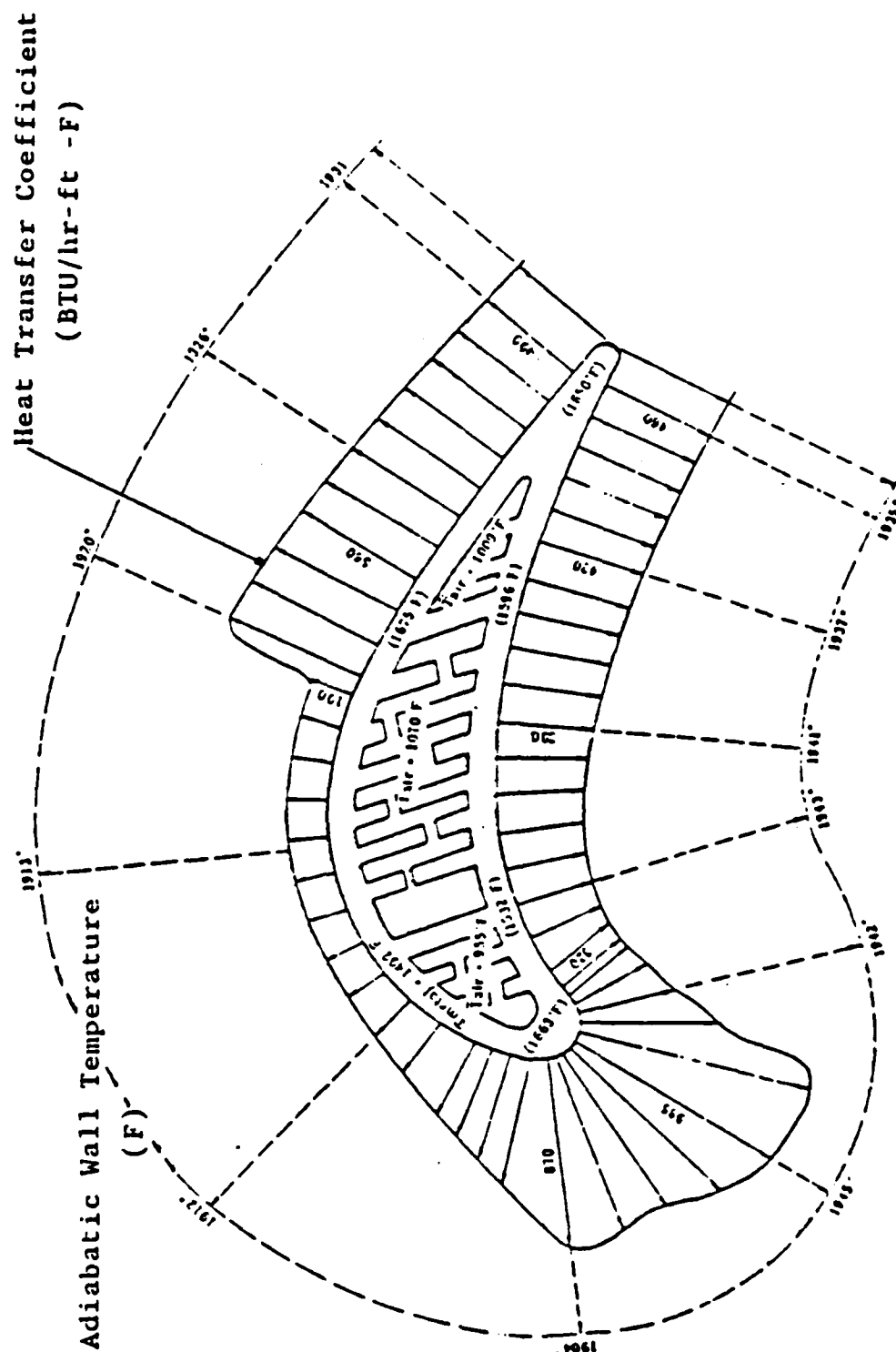


Fig. 8 Film Cooling by a Row of Holes  
with Sample Temperature Profiles.



**Fig. 9 Distribution of Heat Transfer Coefficient and Adiabatic Wall Temperature Around a Typical Blade.**

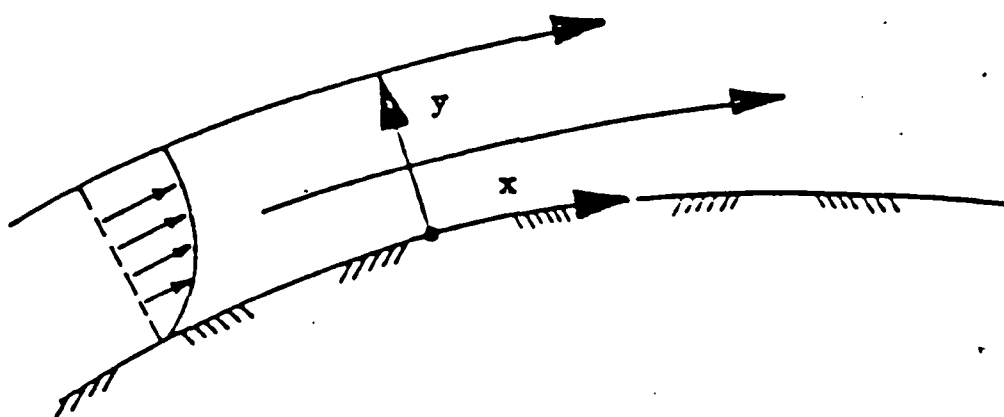


Fig. 10 Curvilinear System of Coordinates.

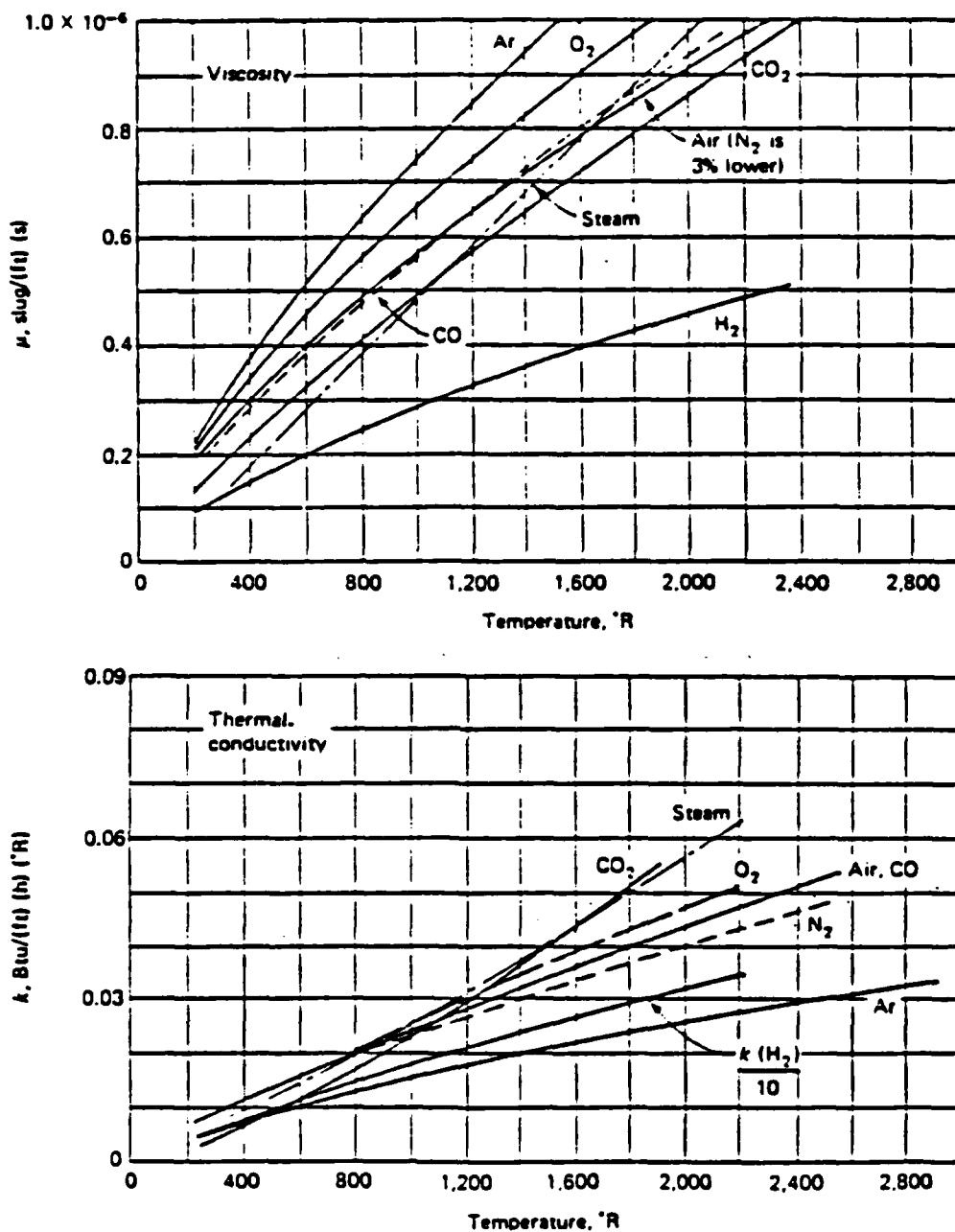


Fig. 11 Viscosity and Thermal Conductivity of Common Gases at Low Pressures.

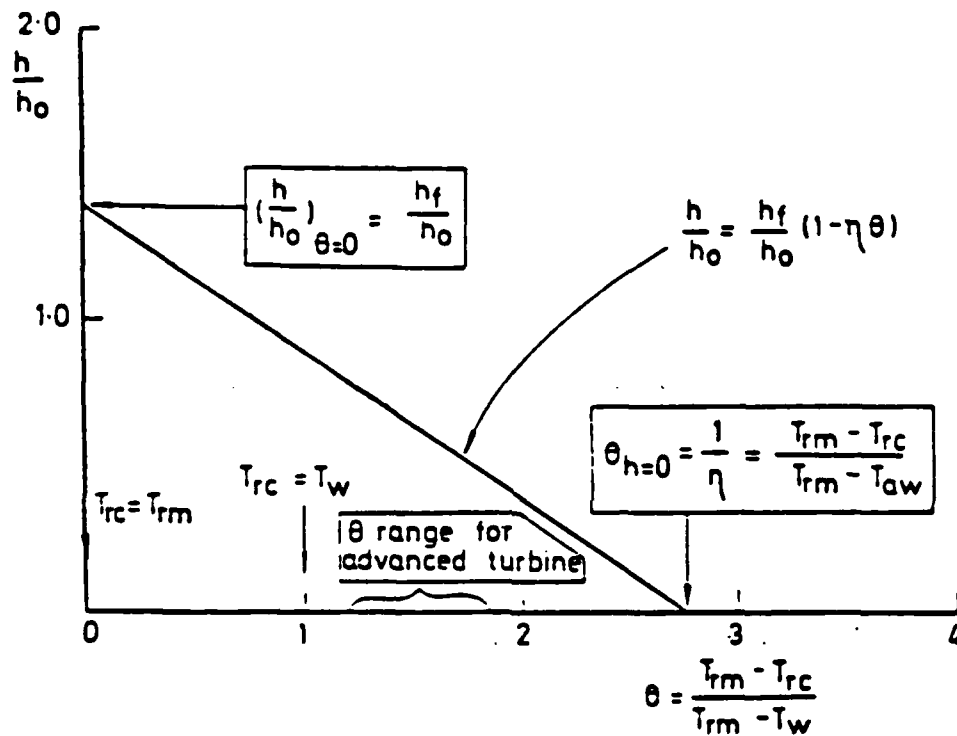


Fig. 12 Linear Variation of Heat Transfer Coefficient with Nondimensional Coolant Temperature.

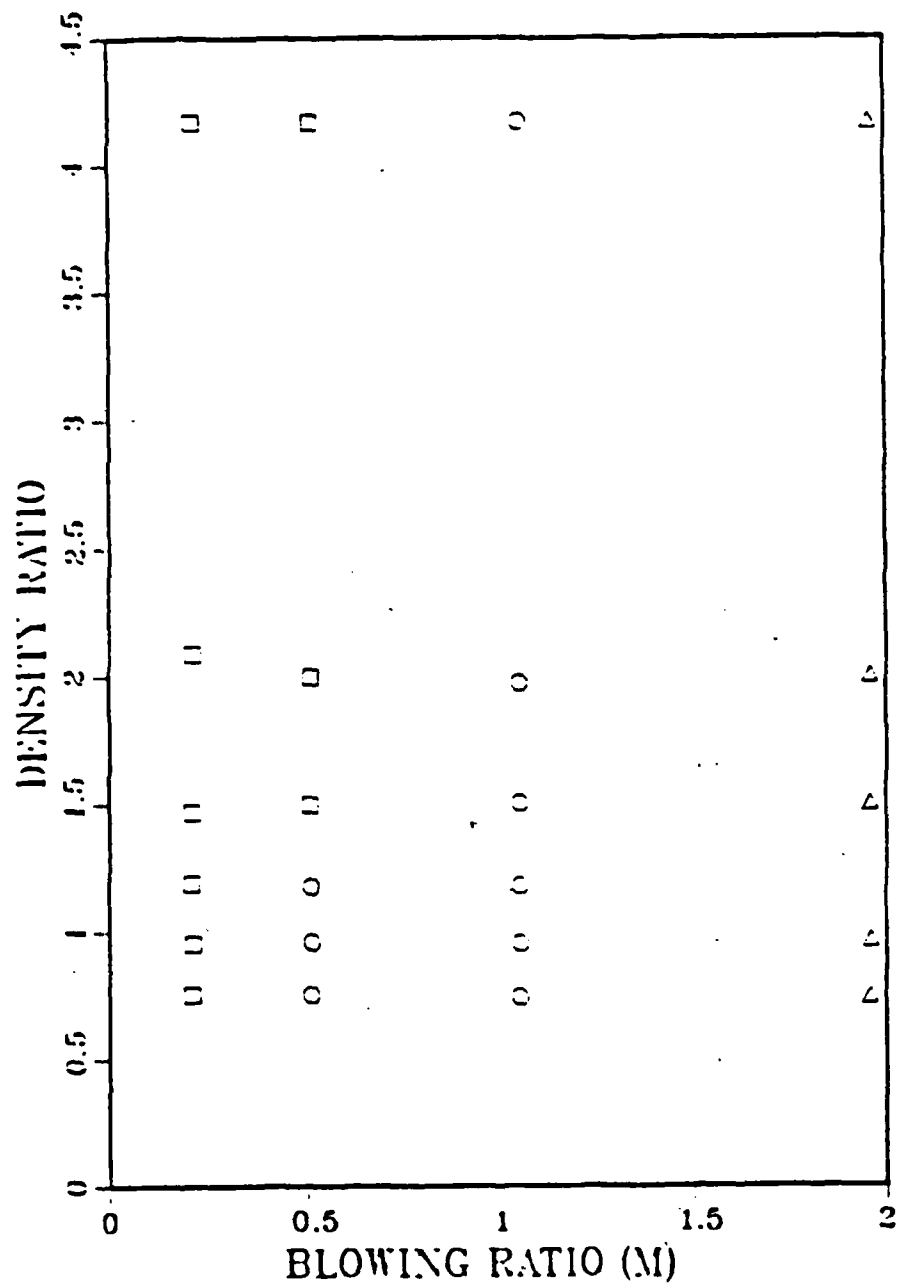


Fig. 13 Domain Map of Blowing Ratio and Density Ratio for Pedersen, Eckert, and Goldstein (1977) Data.



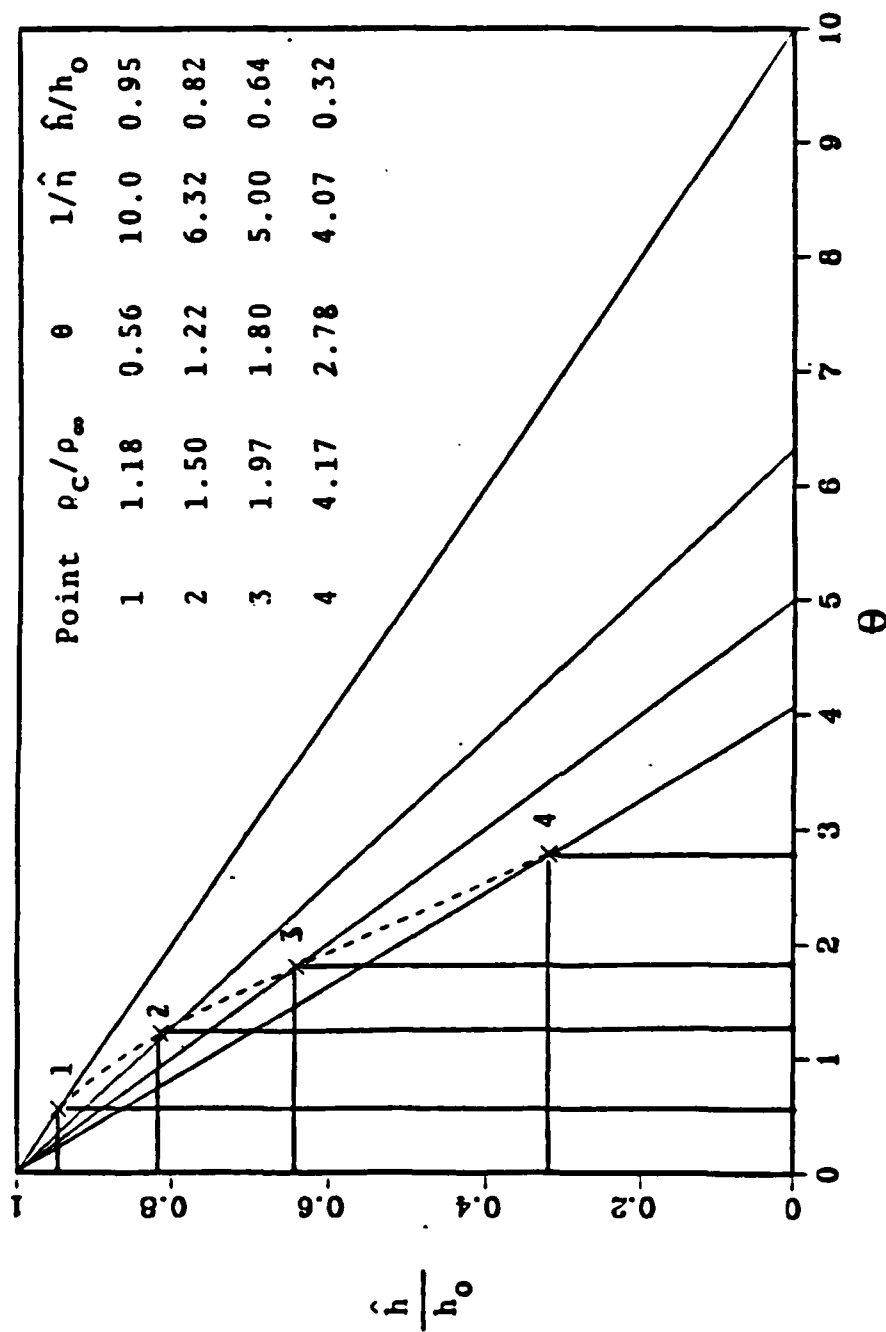


Fig. 14 Nonlinear Variation of  $h/h$  with  $\theta$ .

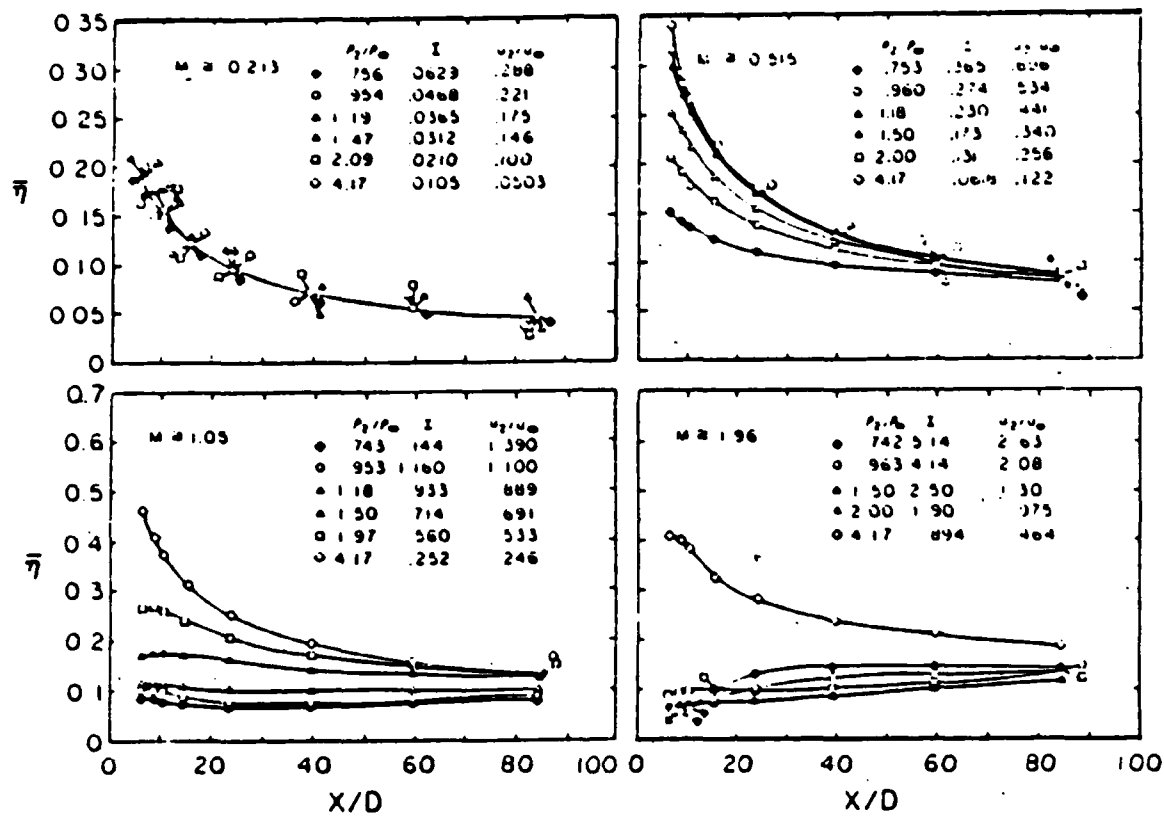


Fig. 15 Effectiveness Verses  $x/d$  from Pedersen, Eckert, and Goldstein (1977).

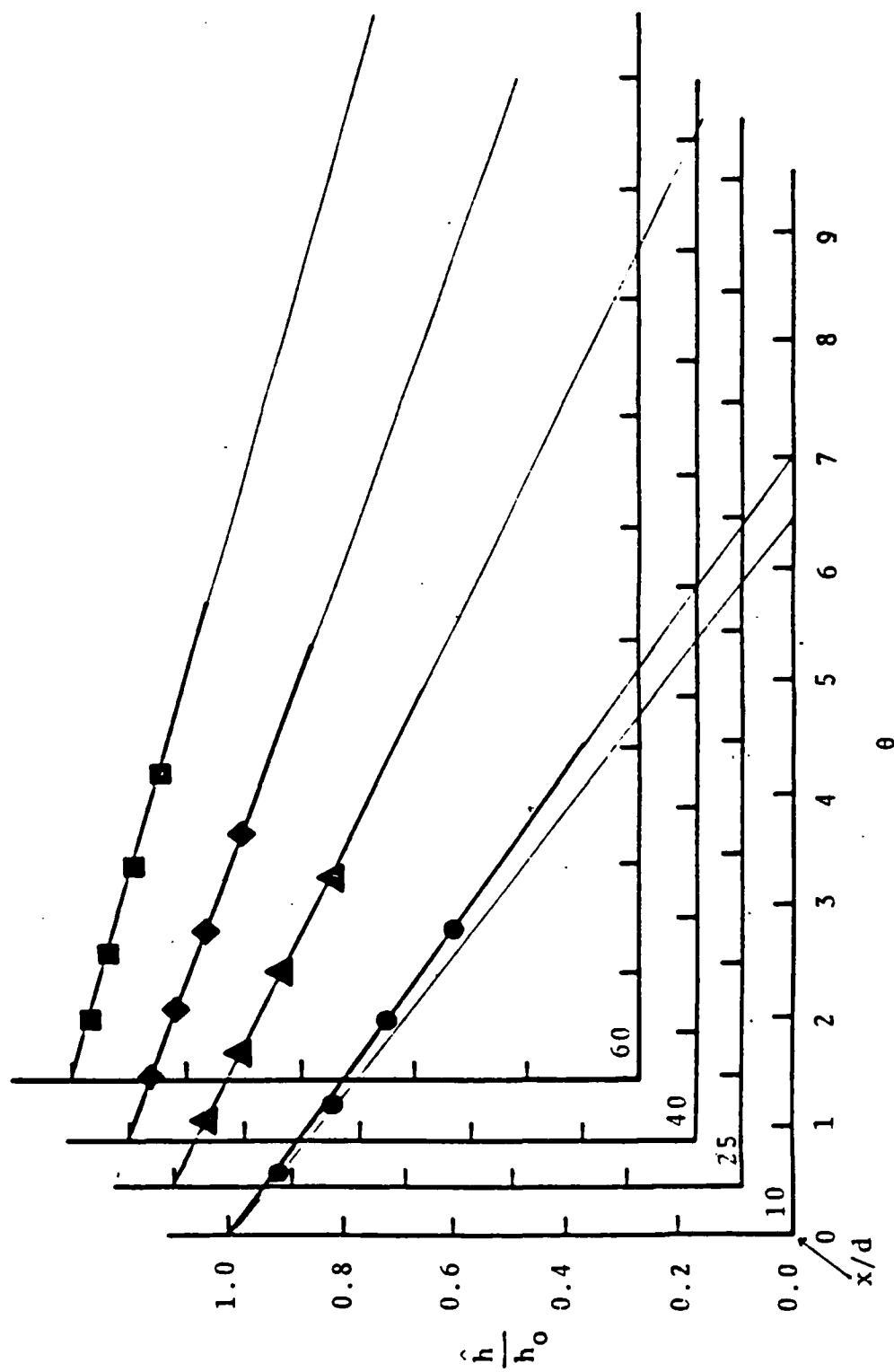


Fig. 16 Variation of  $\hat{h}/h_0$  with  $\theta$  and  $x/d$  for  $M=0.213$ .

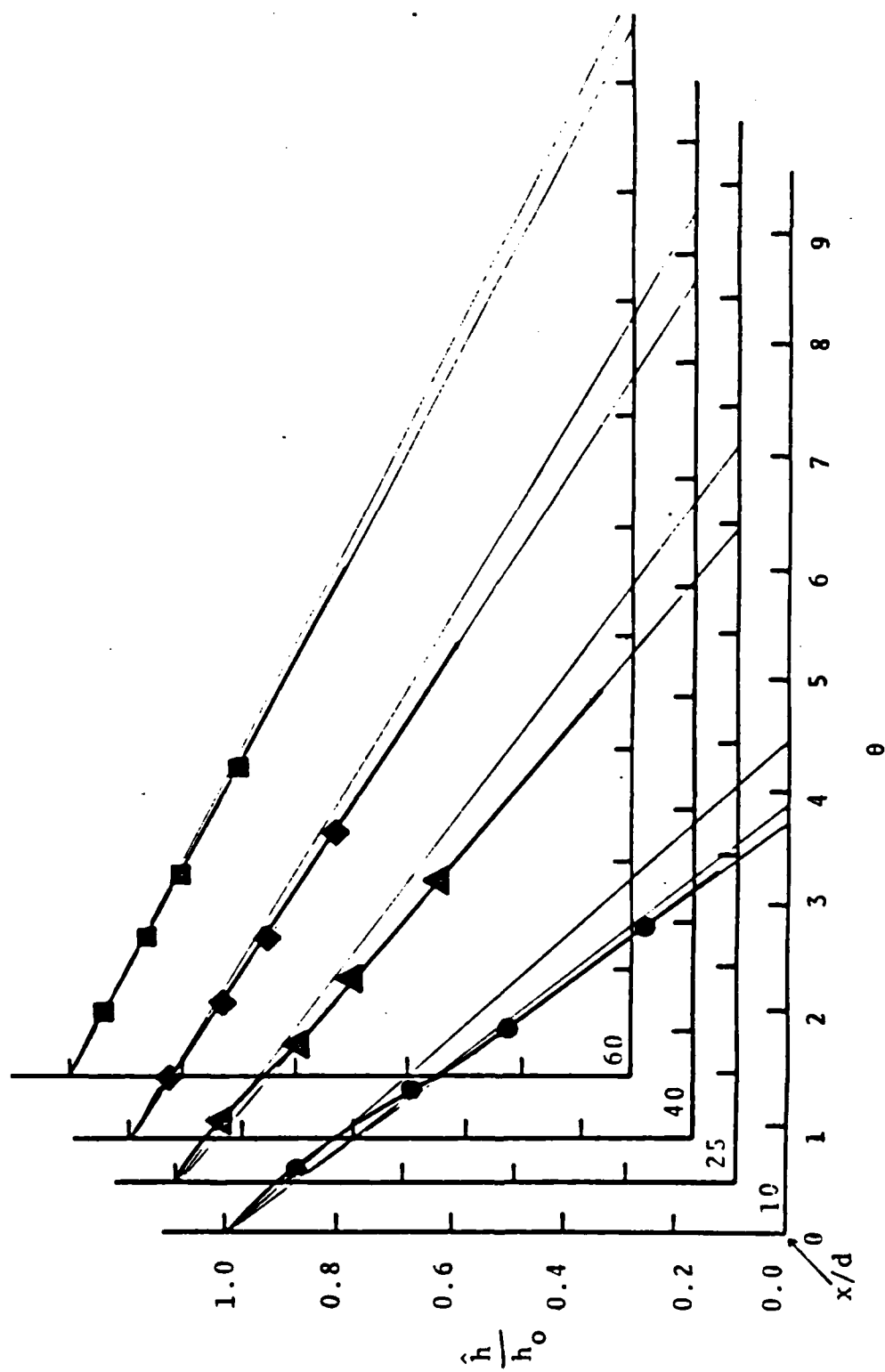


Fig. 17 Variation of  $\hat{h}/h_0$  with  $\theta$  and  $x/d$  for  $M=0.515$ .

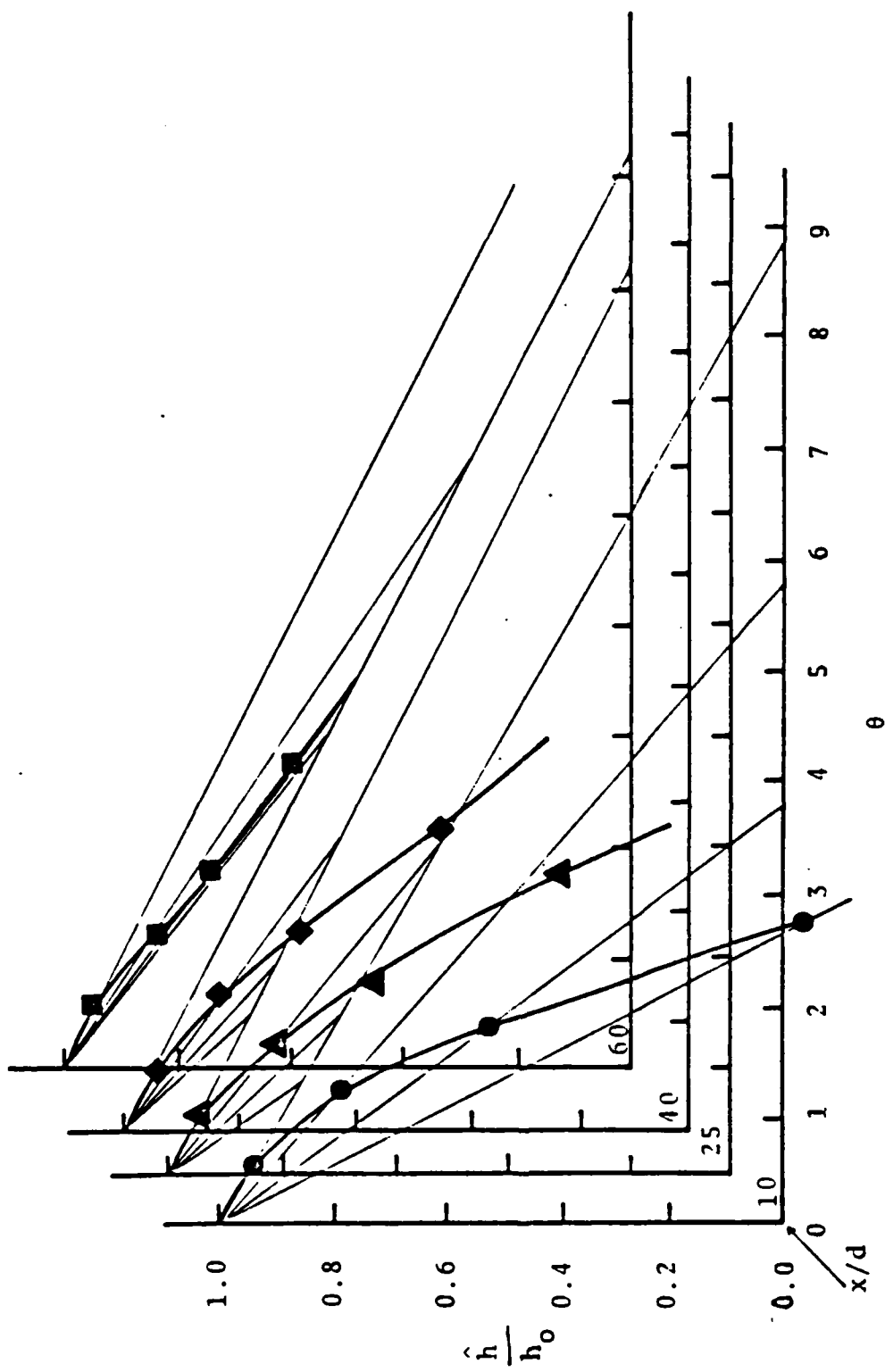


Fig. 18 Variation of  $\frac{h}{h_0}$  with  $\theta$  and  $x/d$  for  $M=1.05$ .

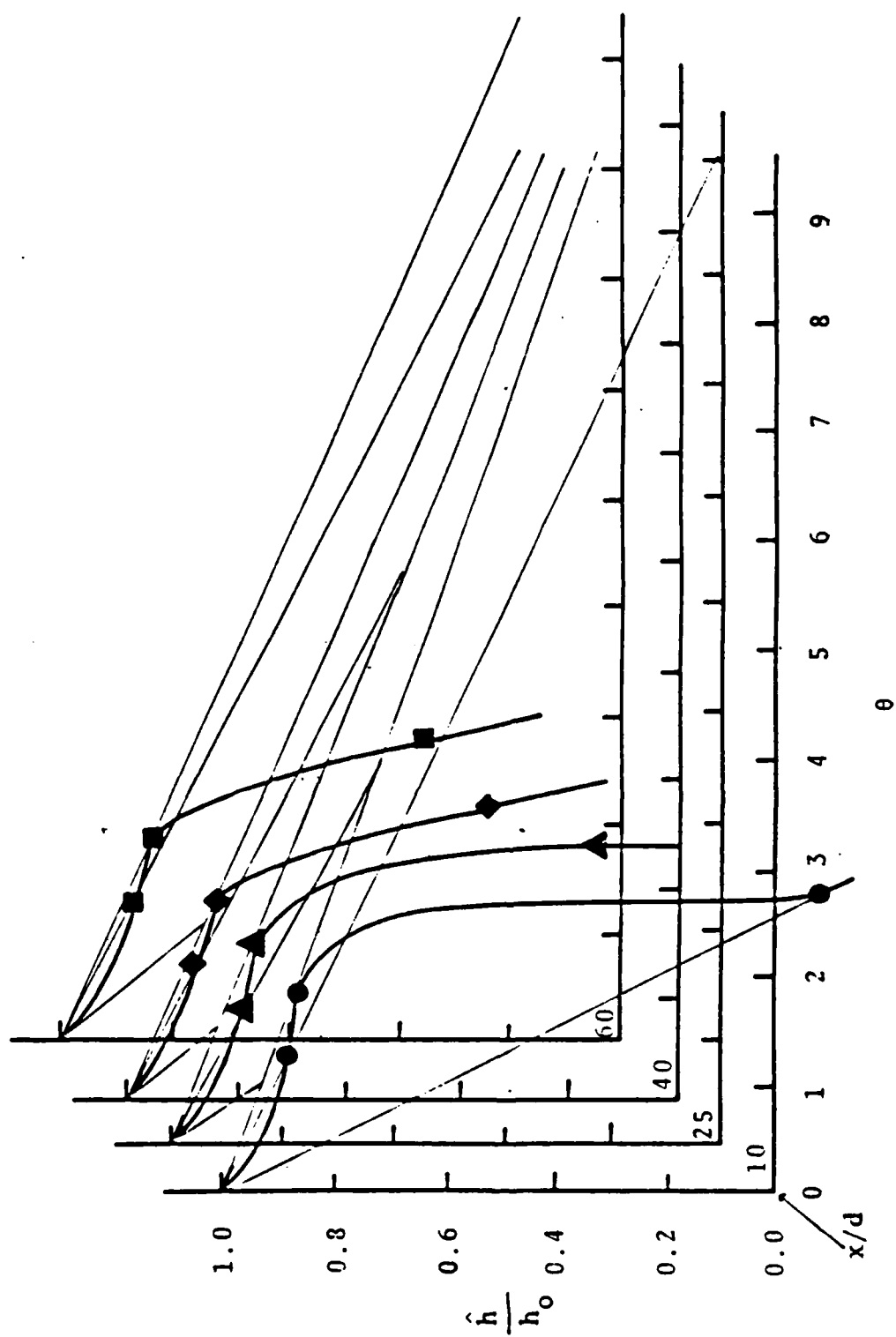


Fig. 19 Variation of  $\hat{h}/h_0$  with  $\theta$  and  $x/d$  for  $M=1.96$ .

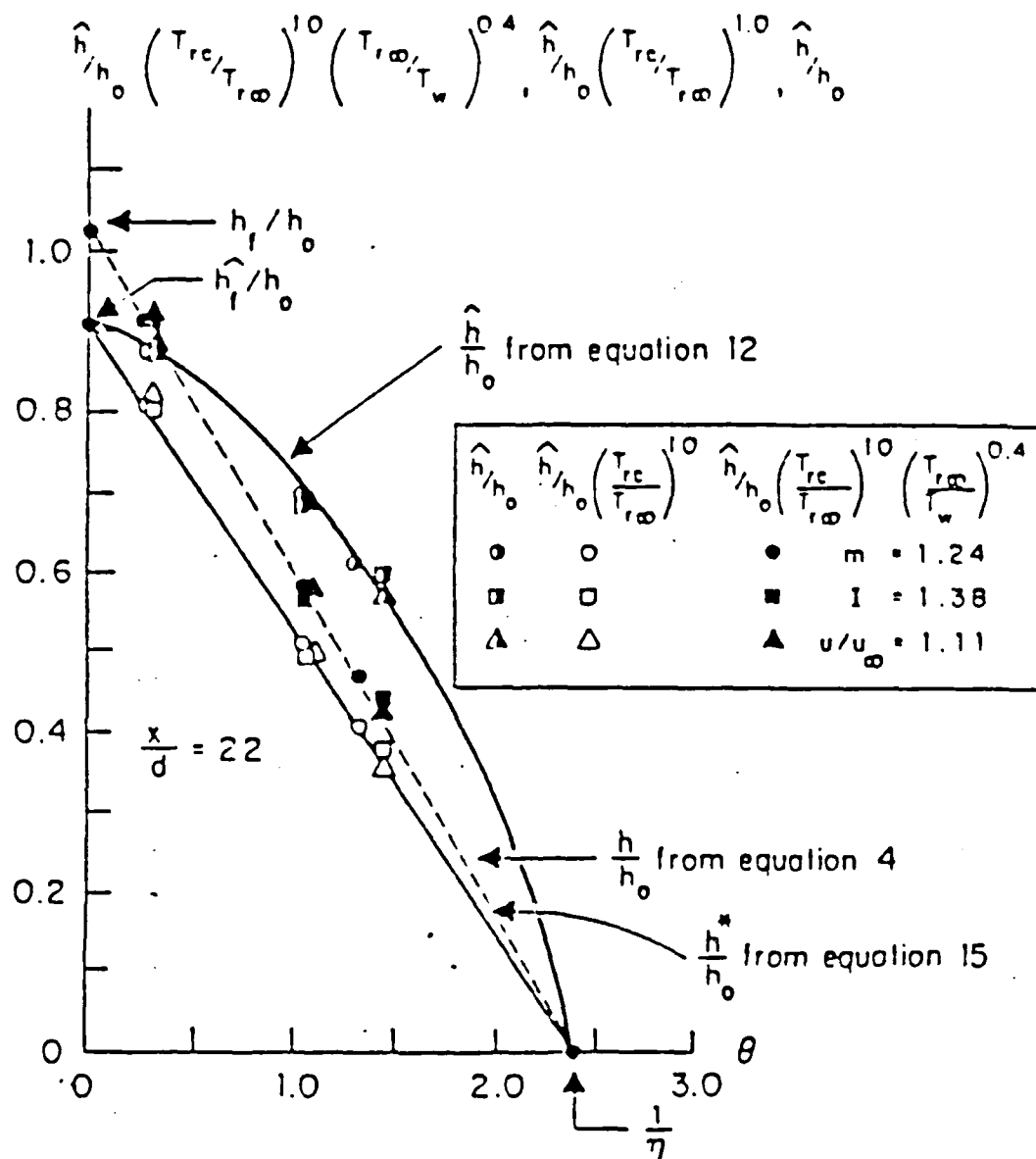


Fig. 20 Variation of  $h/h_o$  with  $\theta$  for Two Rows of Injection from Ligrani and Camci (1985).

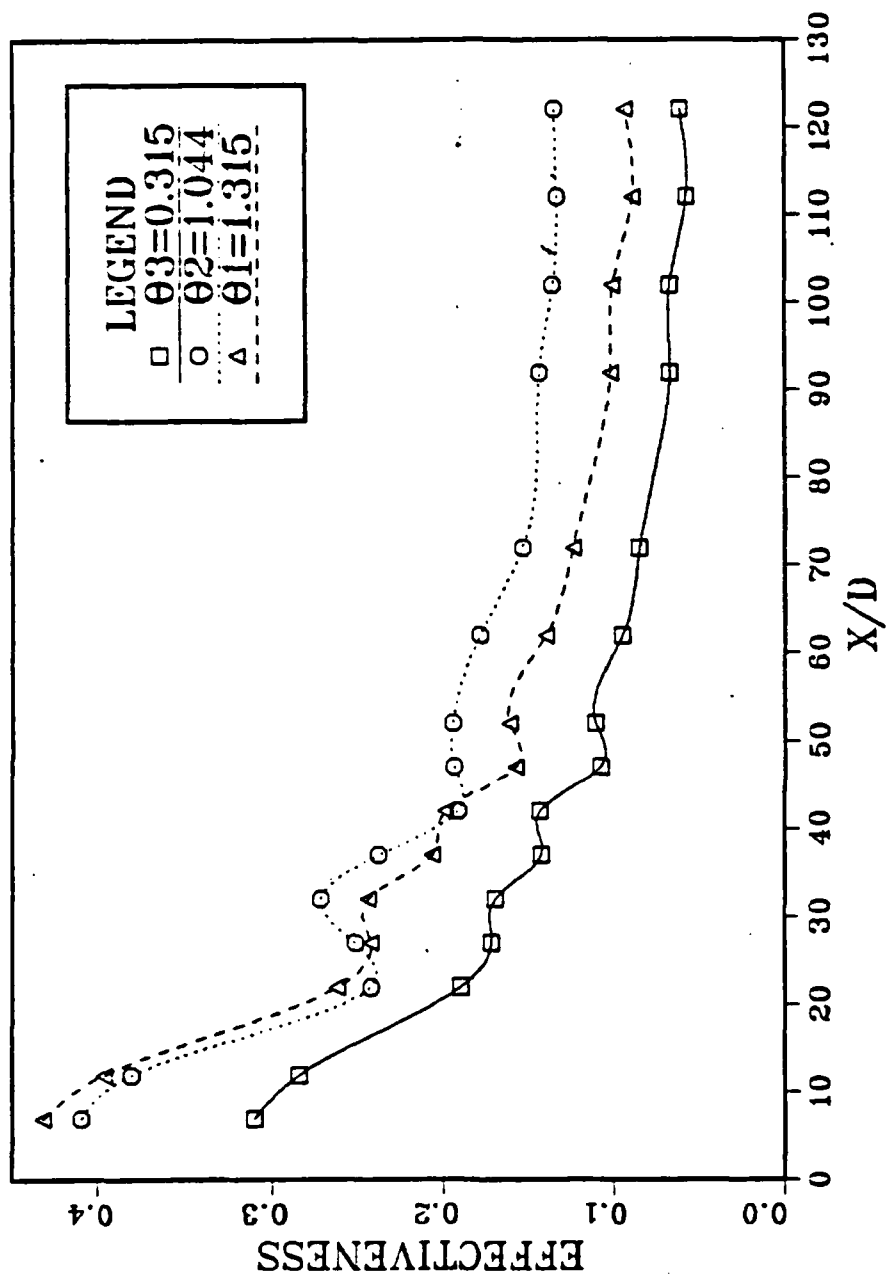


Fig. 21 Variation of  $\hat{\eta}$  with  $x/d$  for  $M=1.242$ .



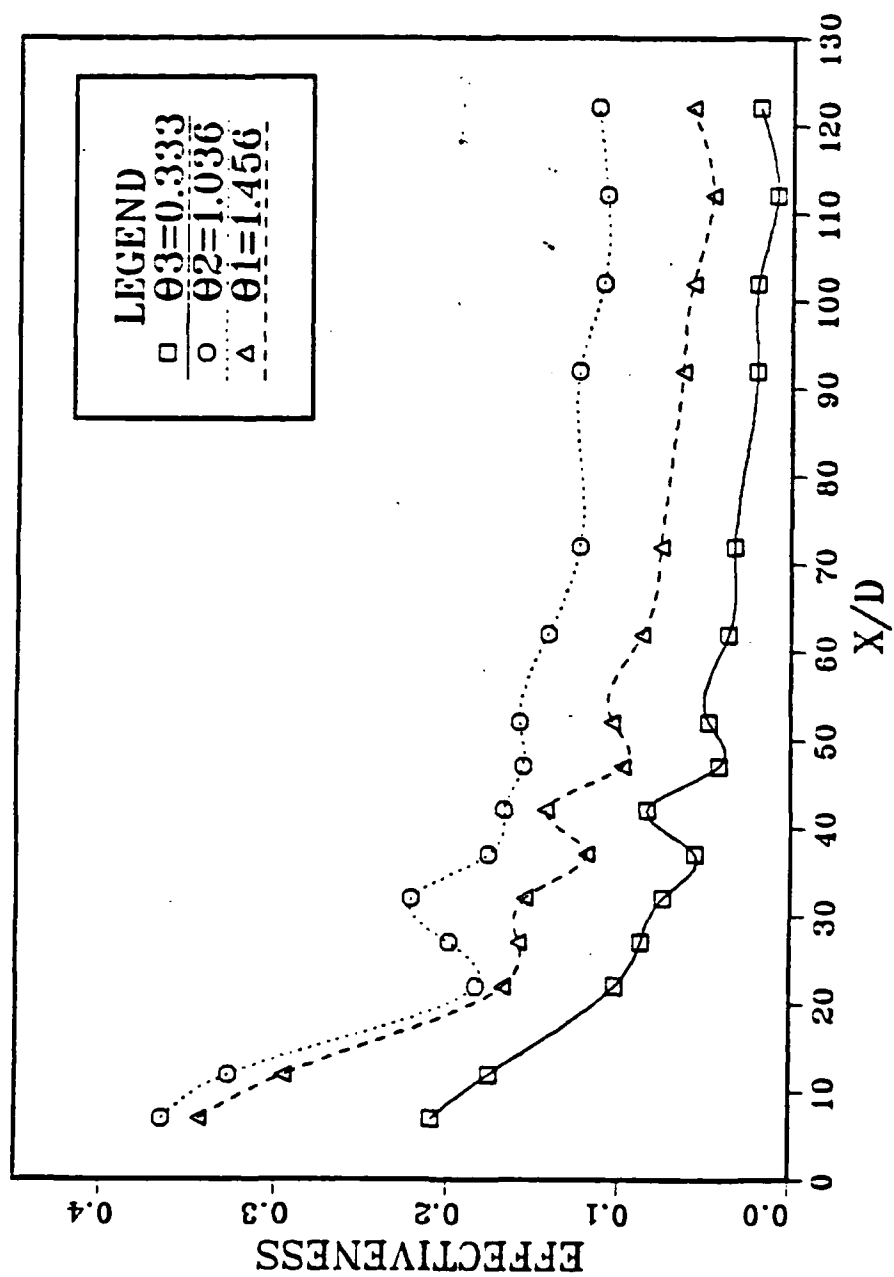


Fig. 22 Variation of  $\hat{n}$  with  $x/d$  for  $M=1.003$ .

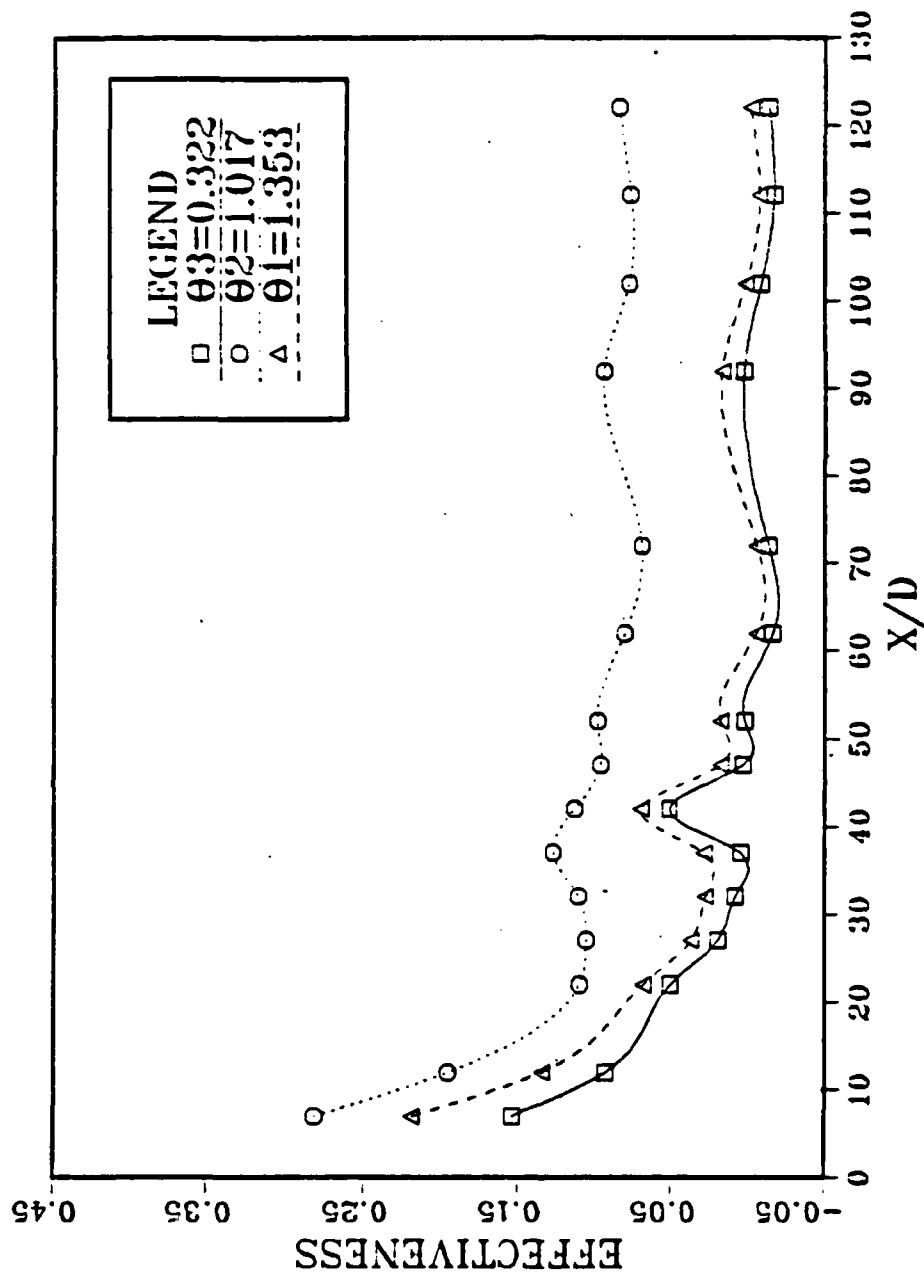


Fig. 23 Variation of  $\hat{\eta}$  with  $x/d$  for  $M=0.481$ .

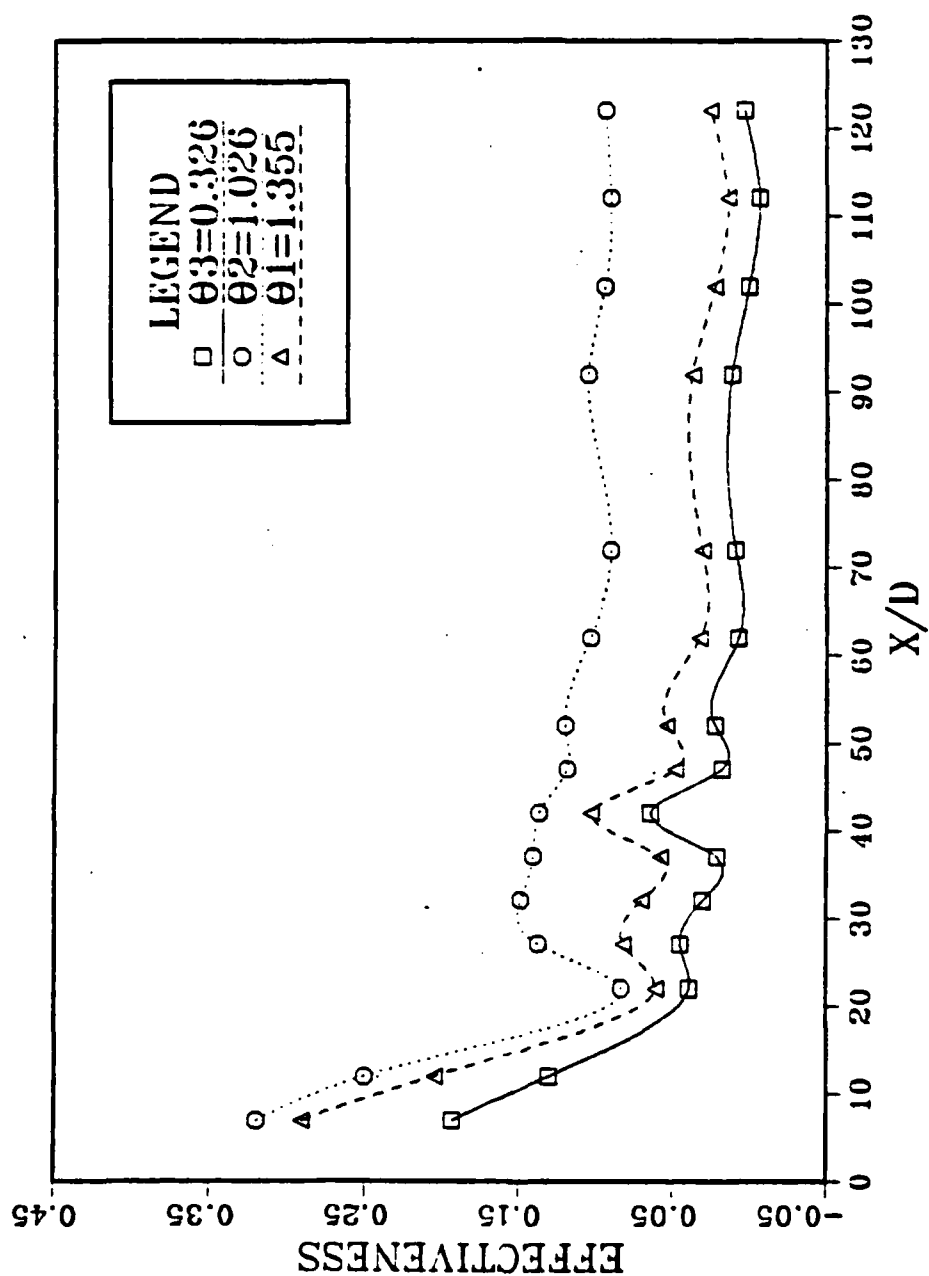


Fig. 24 Variation of  $\hat{\eta}$  with  $x/d$  for  $M=0.661$ .

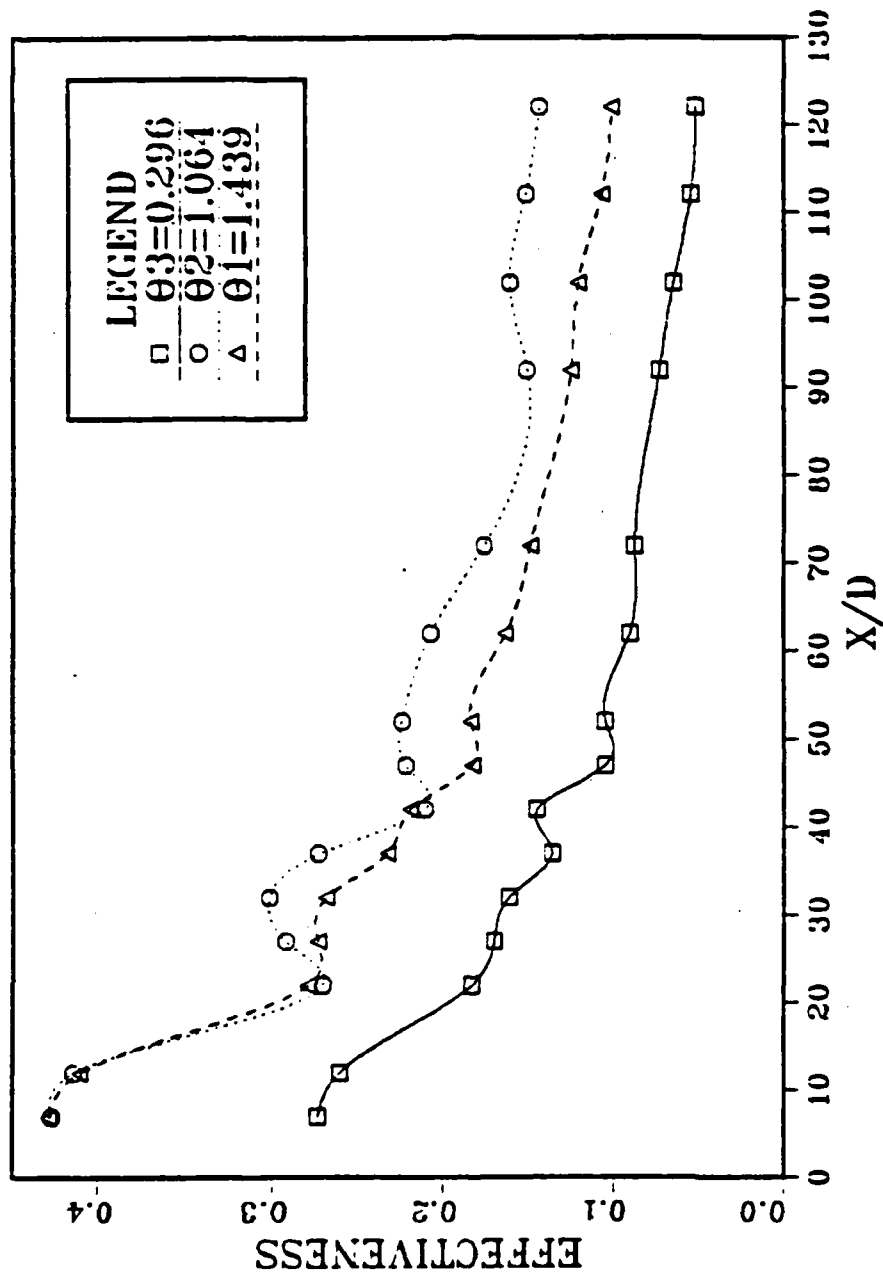


Fig. 25 Variation of  $\hat{\eta}$  with  $x/d$  for  $M=1.557$ .

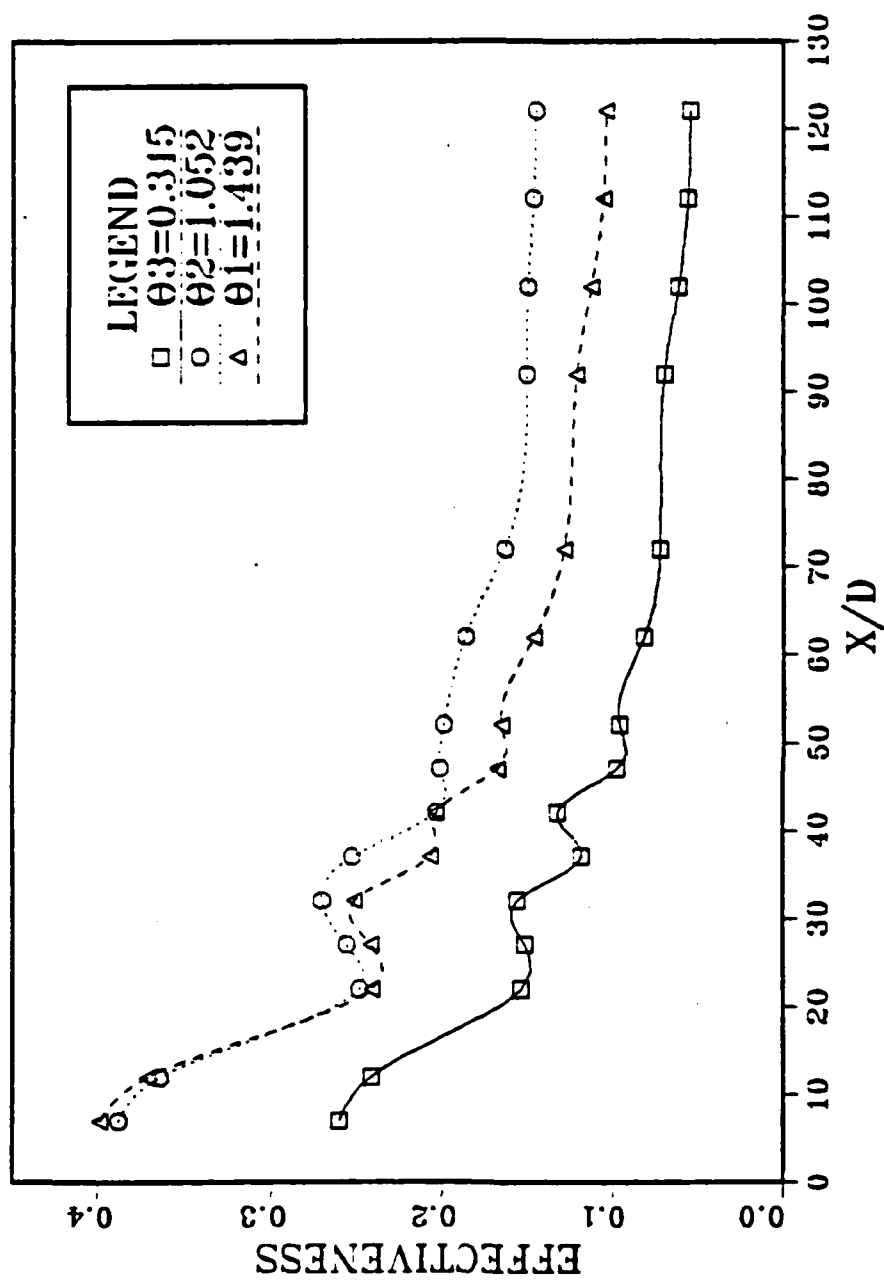


Fig. 26 Variation of  $\hat{\eta}$  with  $x/d$  for  $I=1.382$ .

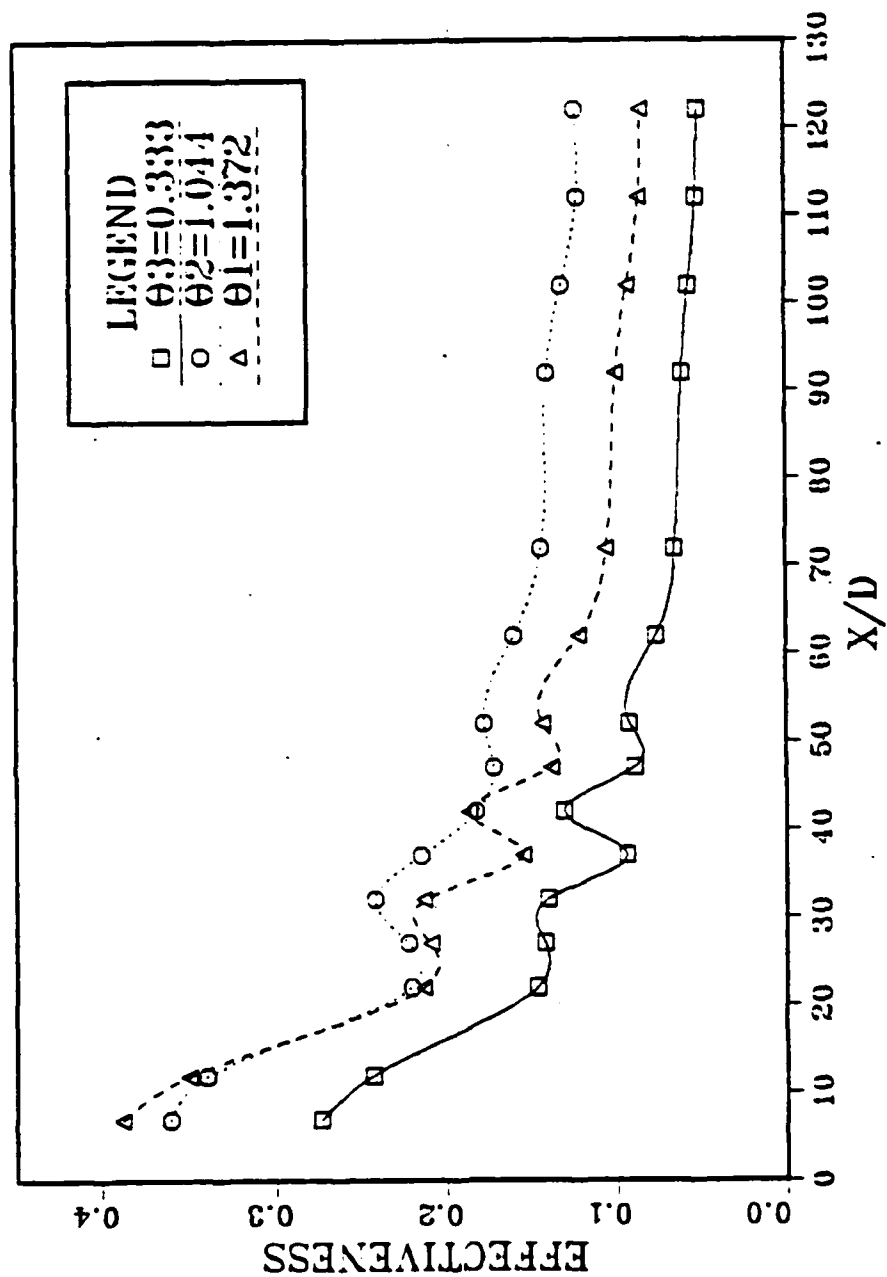


Fig. 27 Variation of  $\hat{\eta}$  with  $x/d$  for  $I=0.925$ .

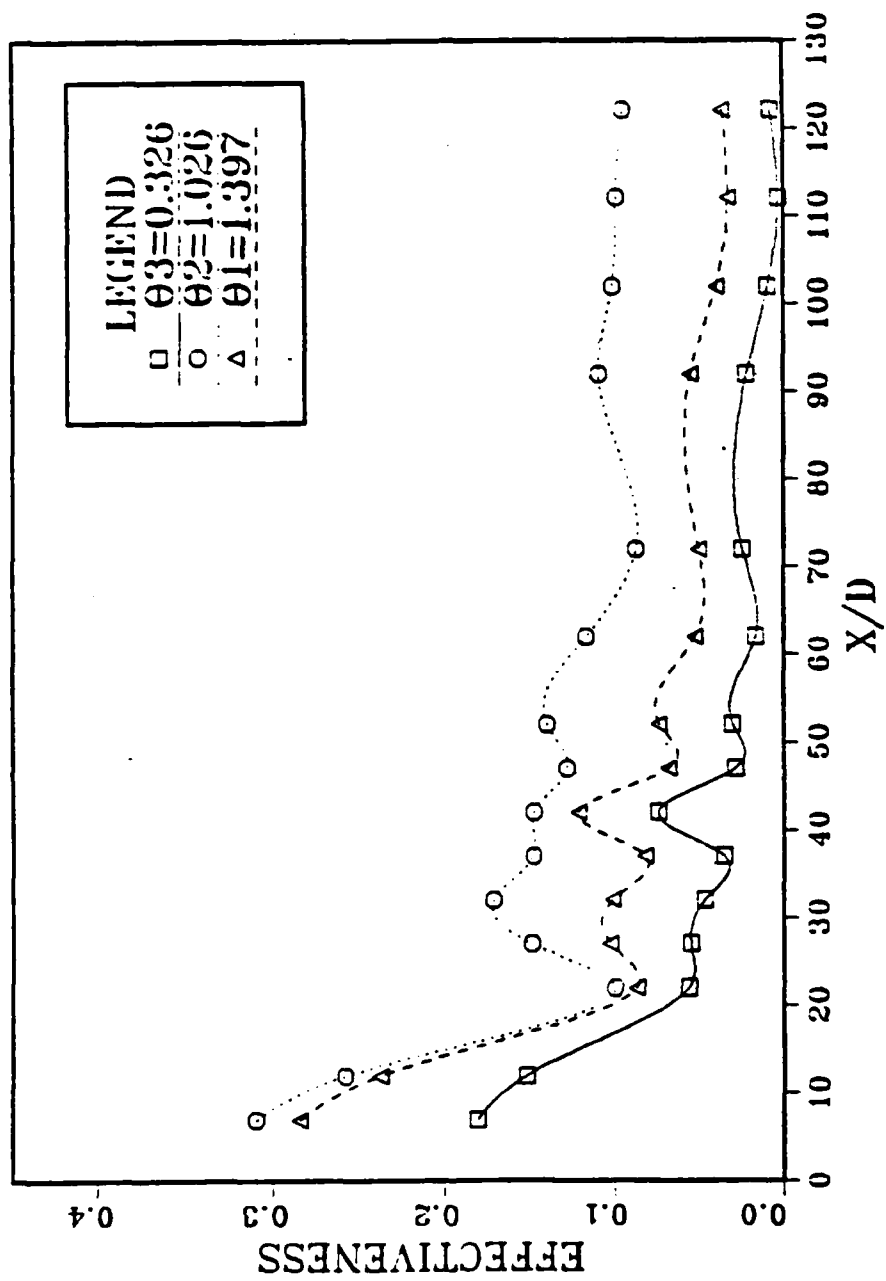


Fig. 28 Variation of  $\hat{\eta}$  with  $x/d$  for  $I=0.417$ .

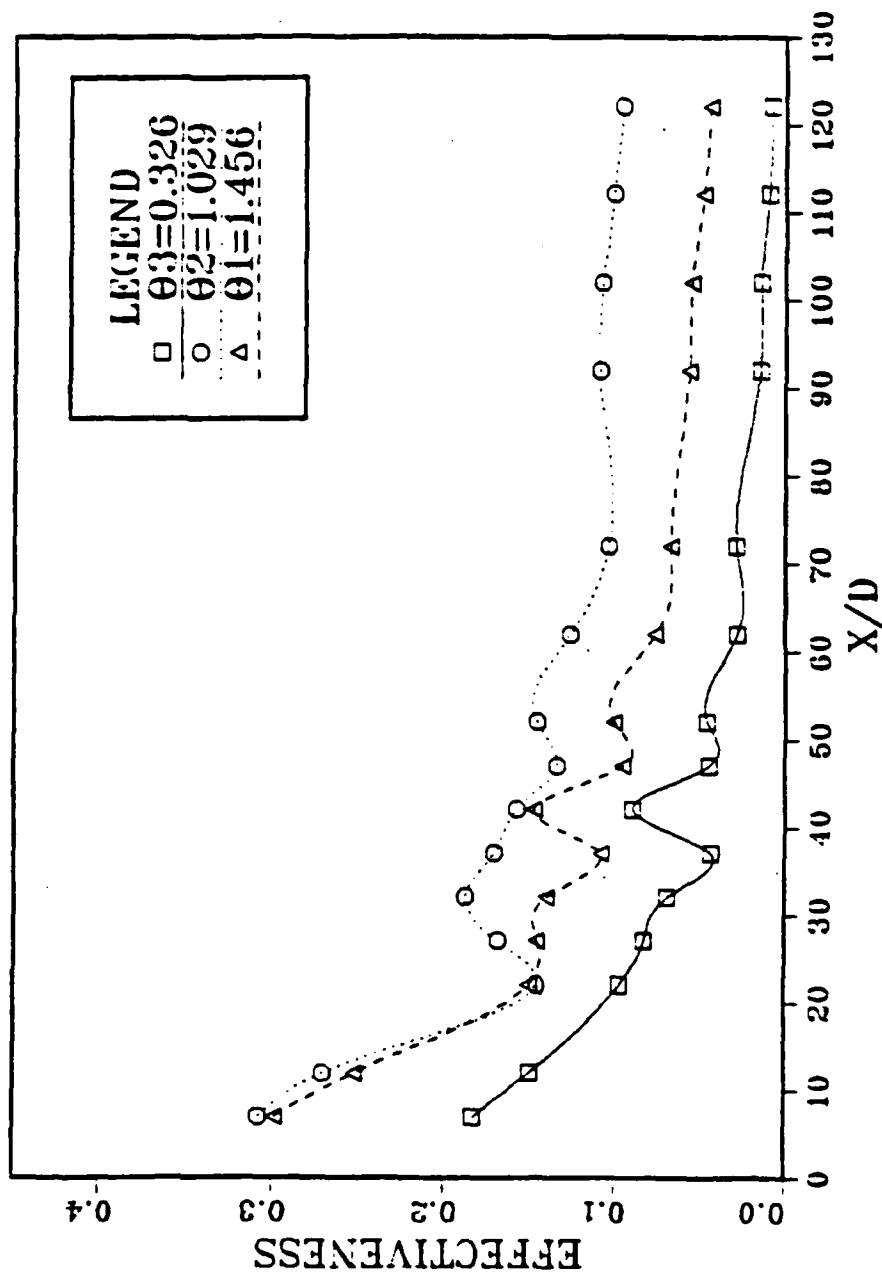


Fig. 29 Variation of  $\hat{\eta}$  with  $x/d$  for  $u_c/u_\infty=0.630$ .



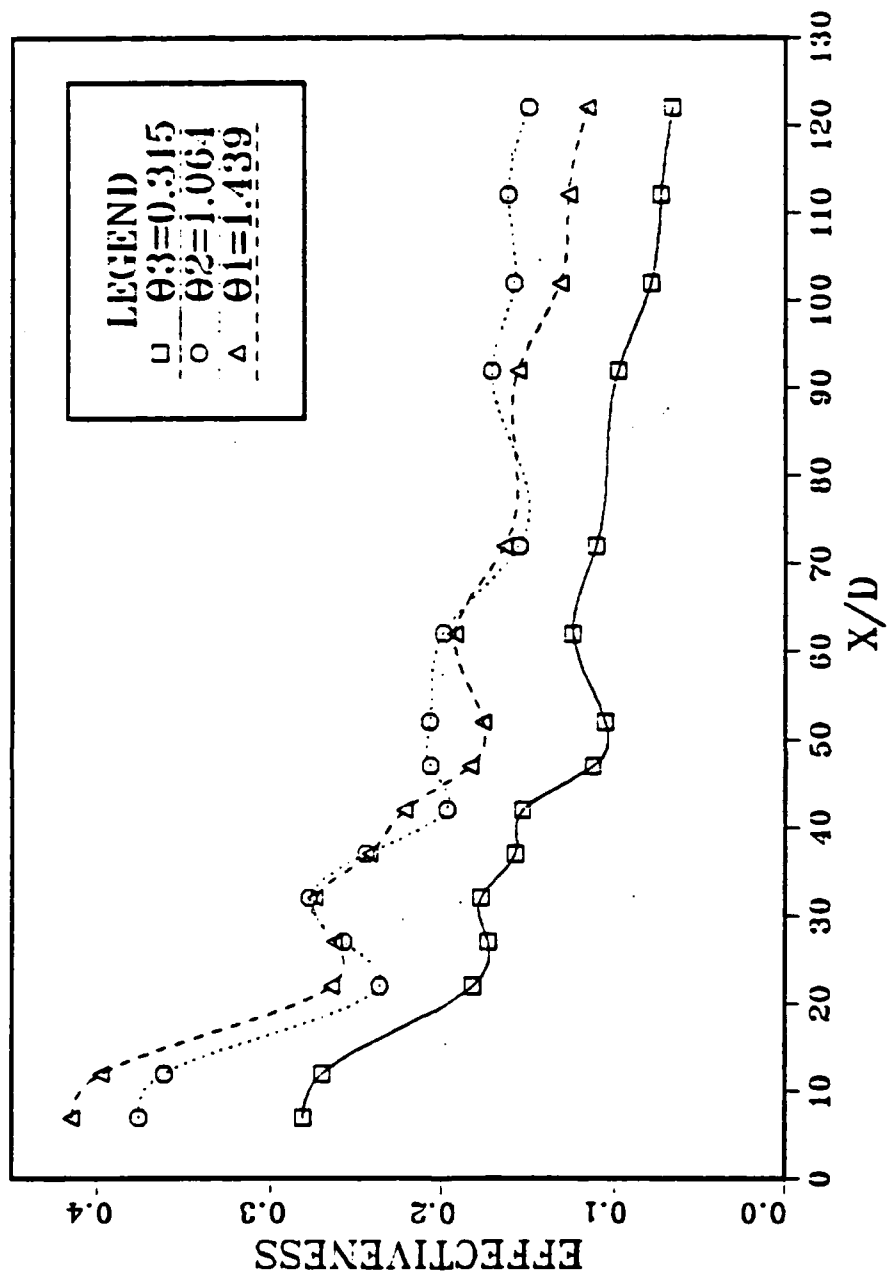


Fig. 30 Variation of  $\hat{\eta}$  with  $x/d$  for  $u_c/u_\infty=1.113$ .

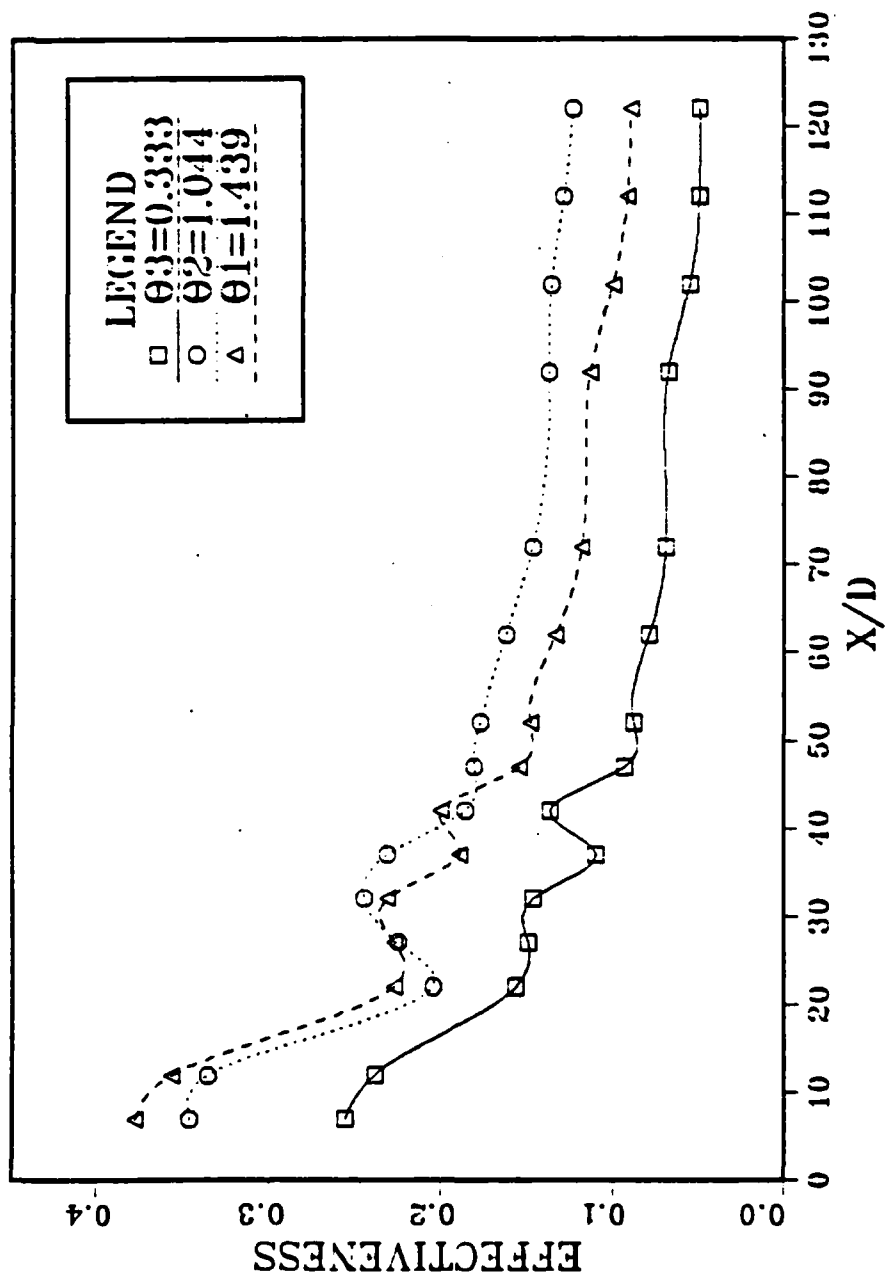


Fig. 31 Variation of  $\hat{\eta}$  with  $x/d$  for  $u_c/u_\infty = 0.922$ .

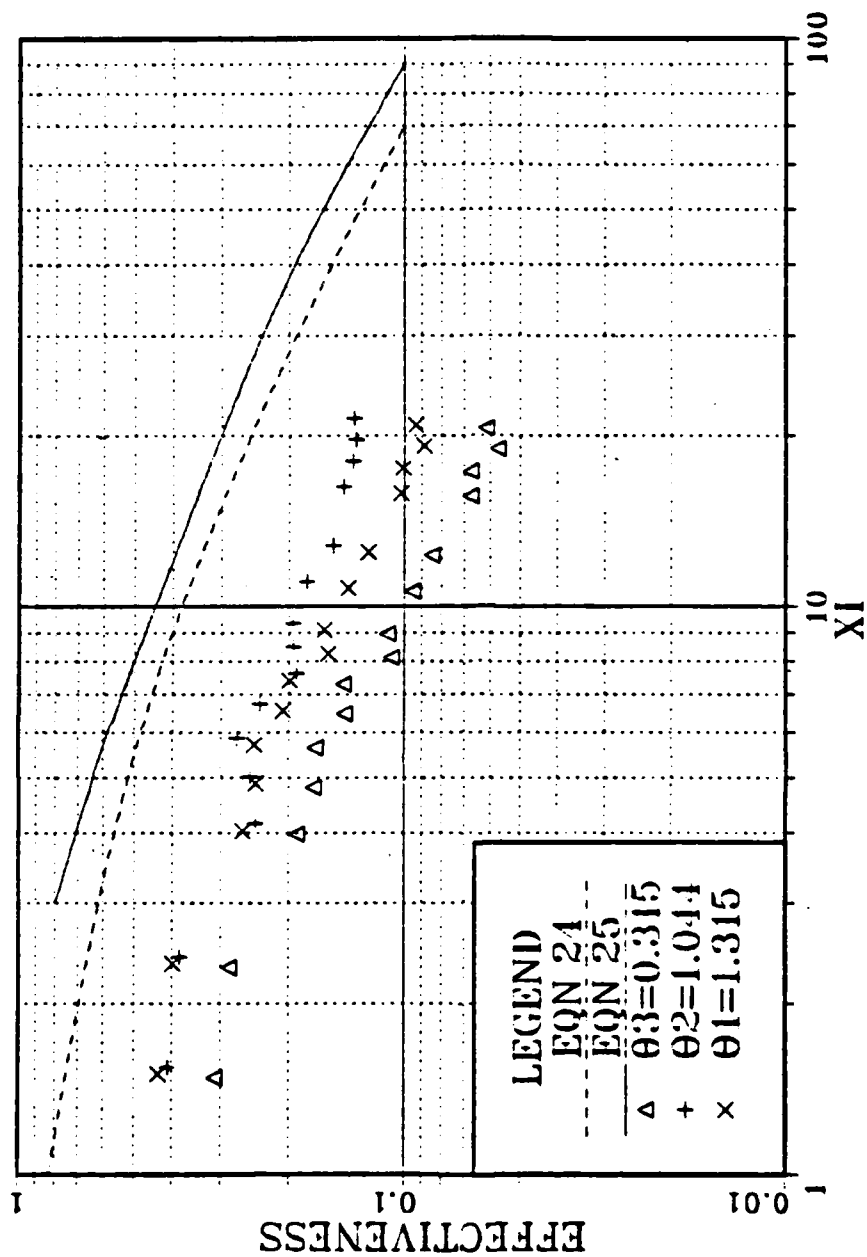


Fig. 32 Variation of  $\hat{\eta}$  with  $\xi$  for  $M=1.242$ .

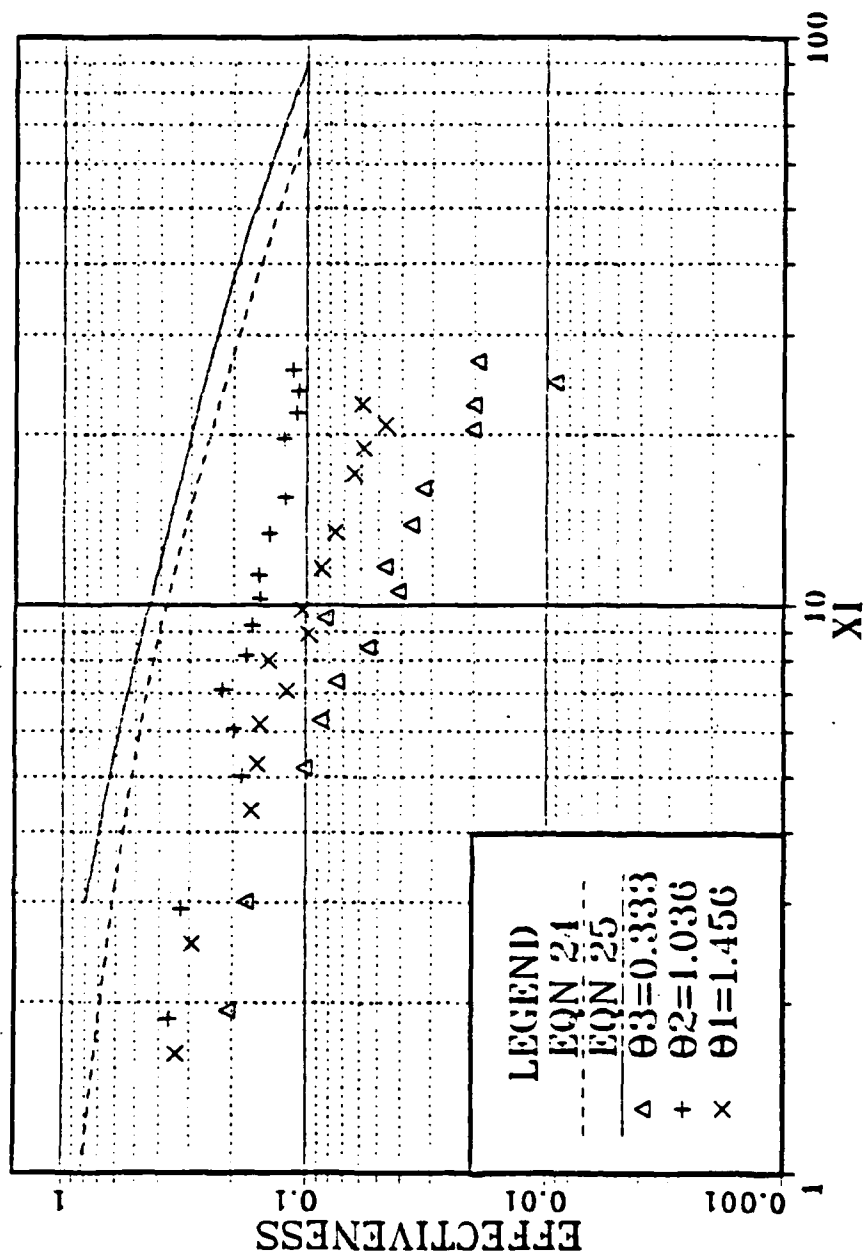


Fig. 33 Variation of  $\hat{\eta}$  with  $\xi$  for  $M=1.003$ .

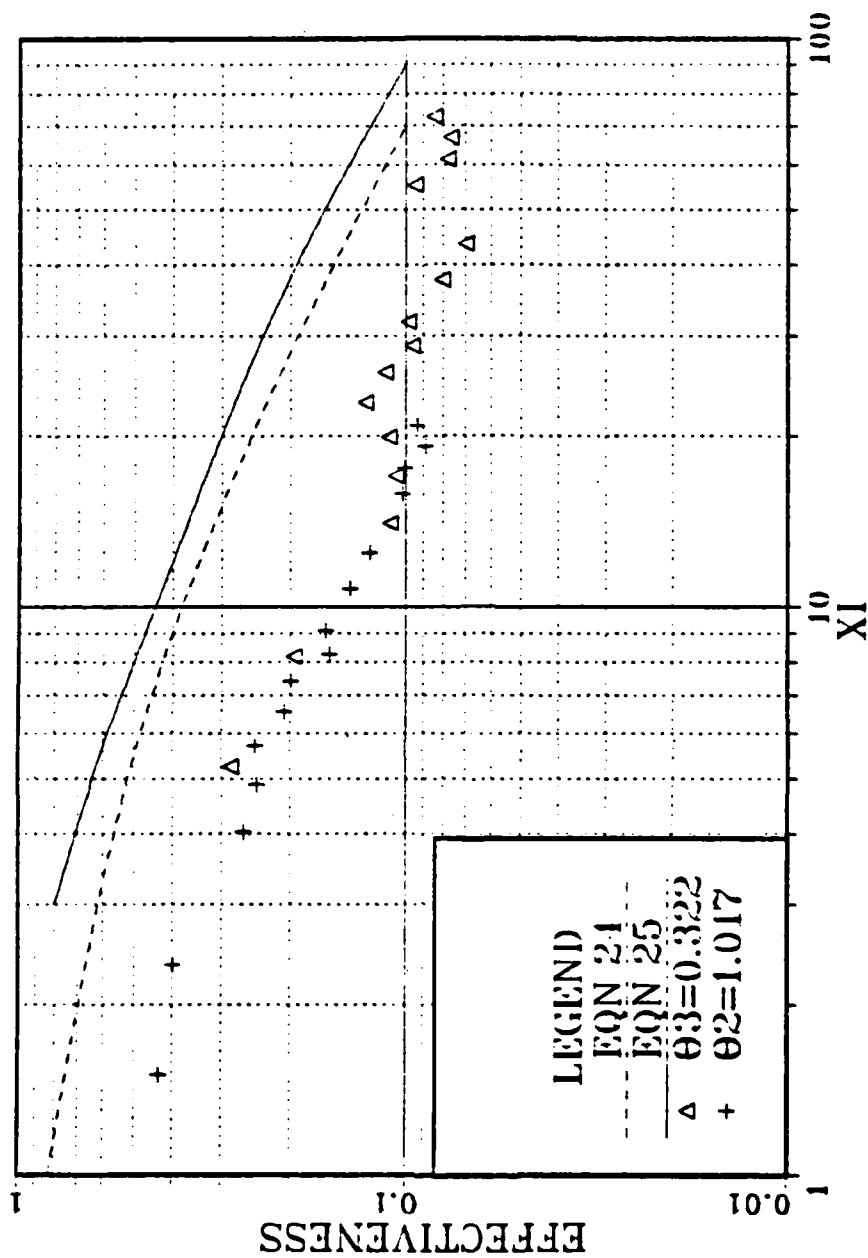


Fig. 34 Variation of  $\hat{\eta}$  with  $\xi$  for  $M=0.481$ .

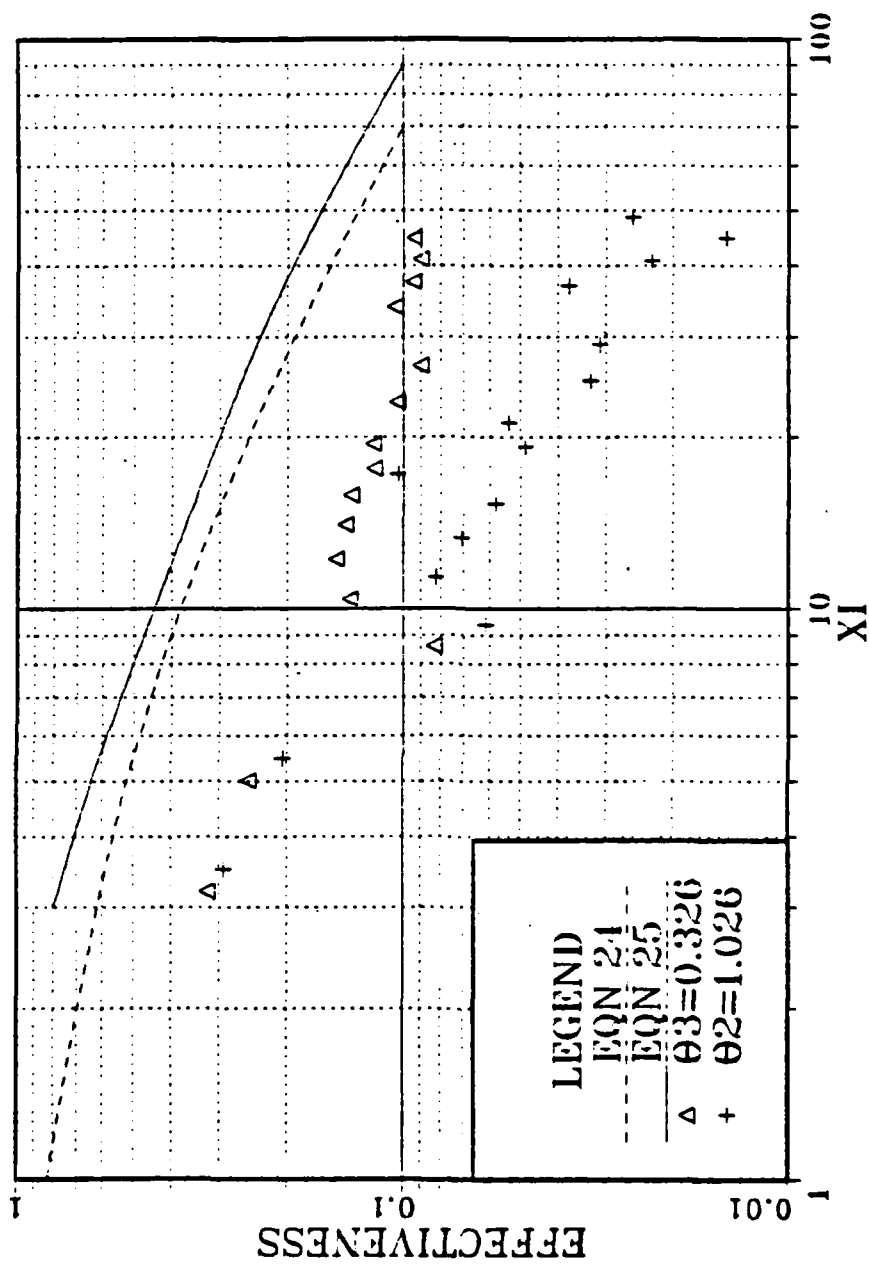


Fig. 35 Variation of  $\hat{\eta}$  with  $\xi$  for  $M=0.661$ .

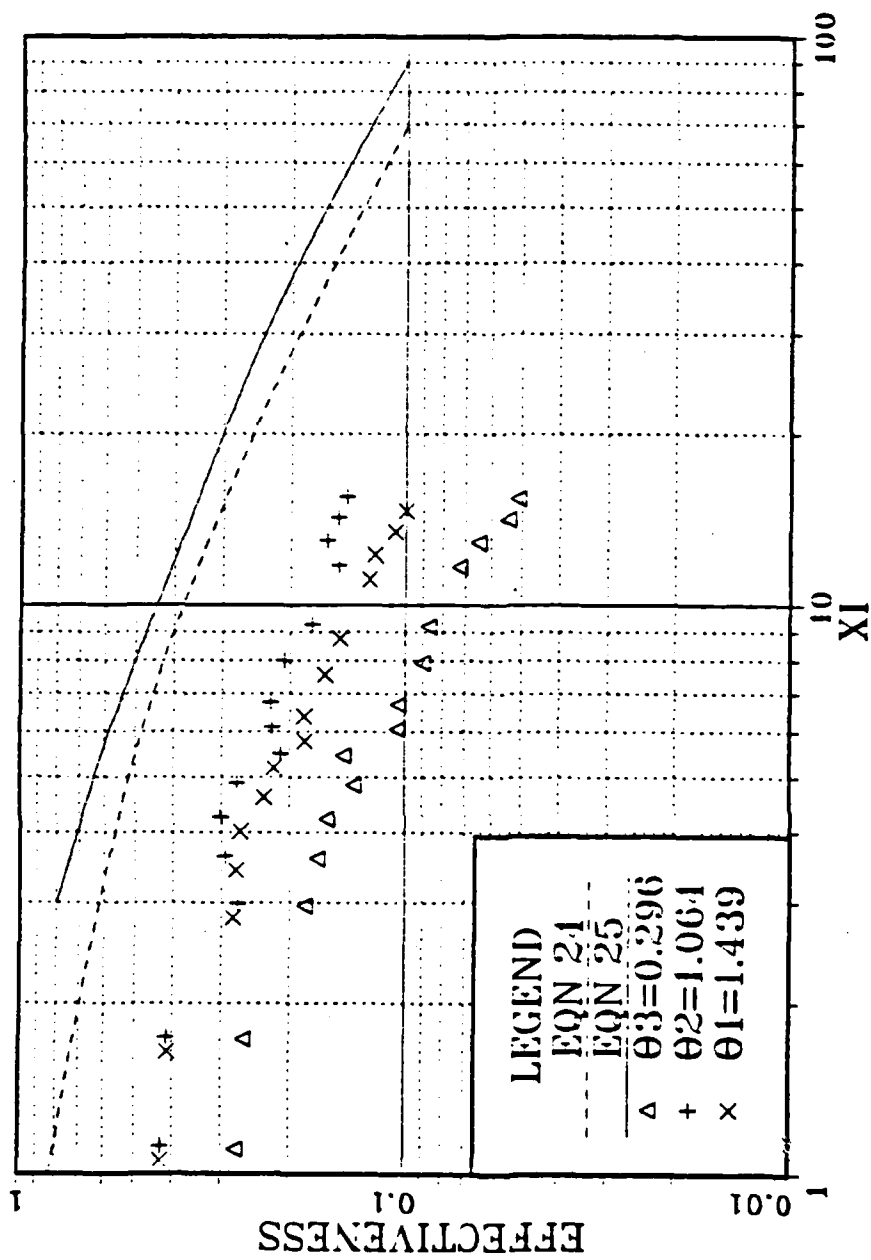


Fig. 36 Variation of  $\hat{n}$  with  $\xi$  for  $M=1.557$ .

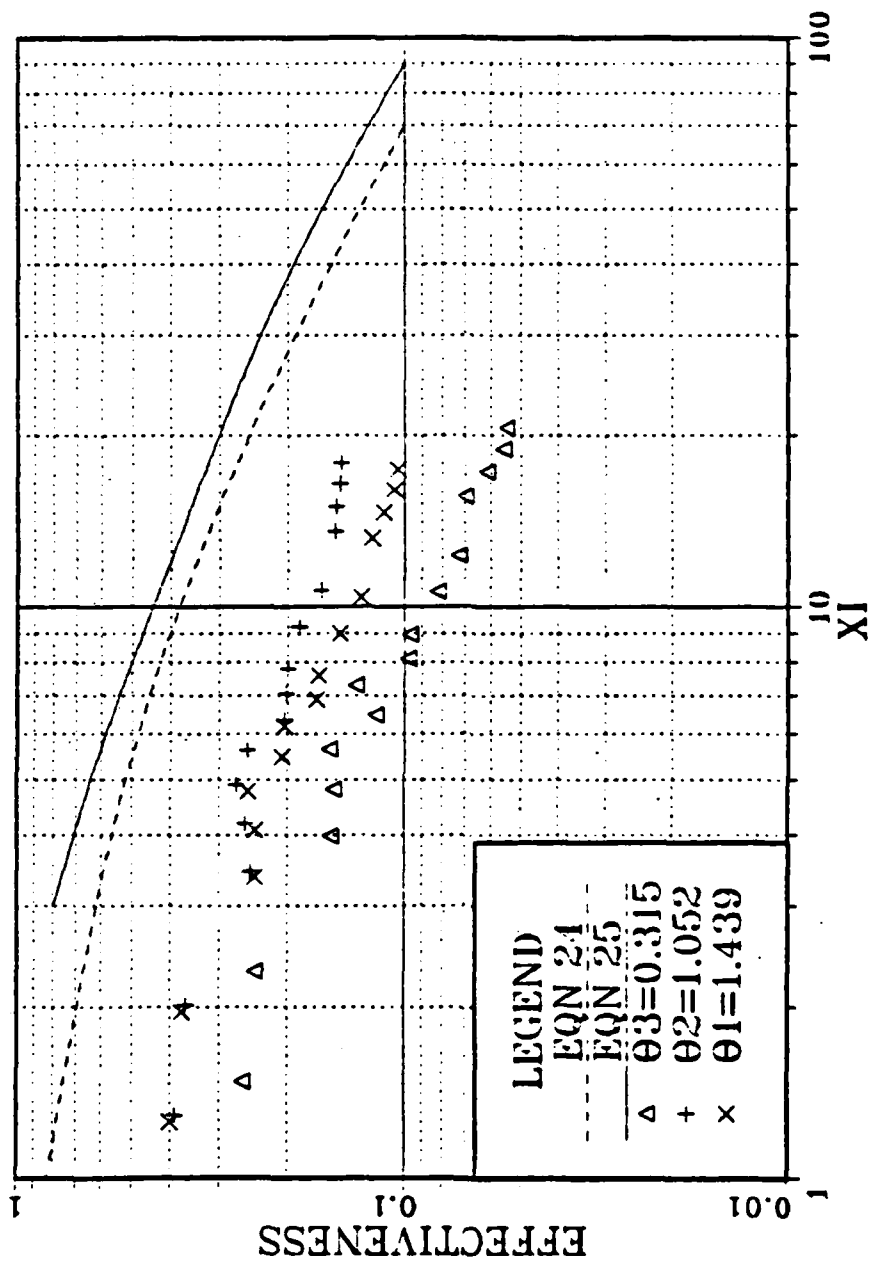


Fig. 37 Variation of  $\hat{\eta}$  with  $\xi$  for  $I=1.382$ .



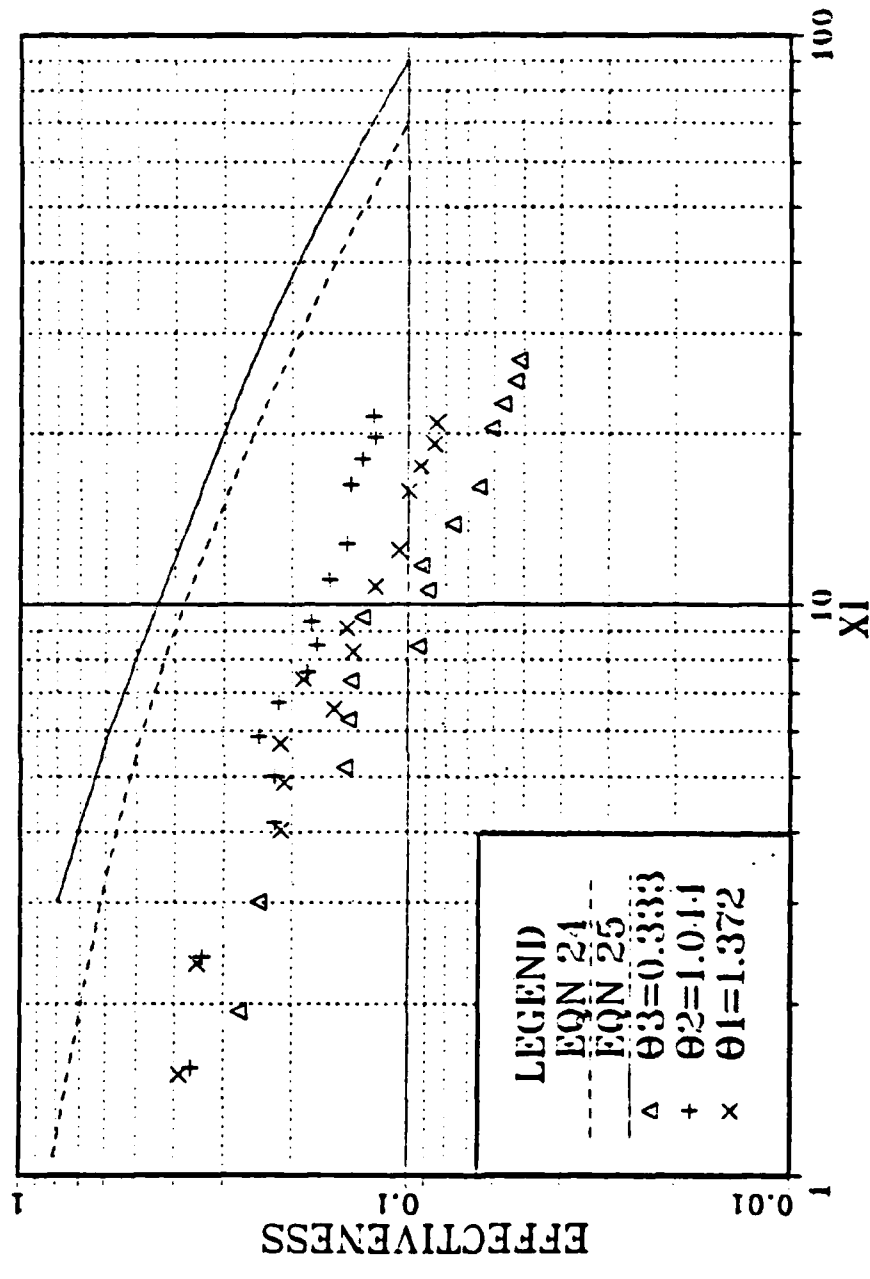


Fig. 38 Variation of  $\hat{\eta}$  with  $\xi$  for  $I=0.925$ .

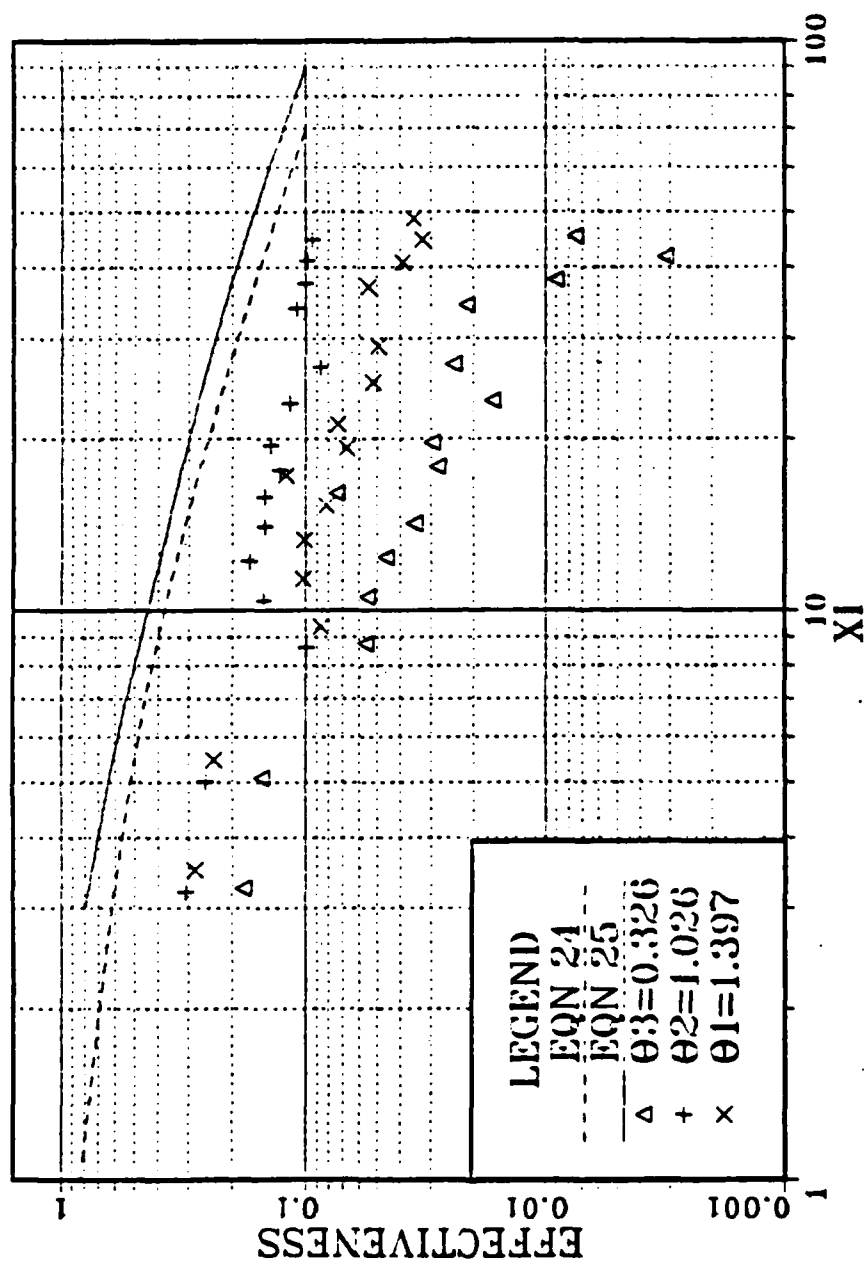


Fig. 39 Variation of  $\hat{\eta}$  with  $\xi$  for  $I=0.417$ .

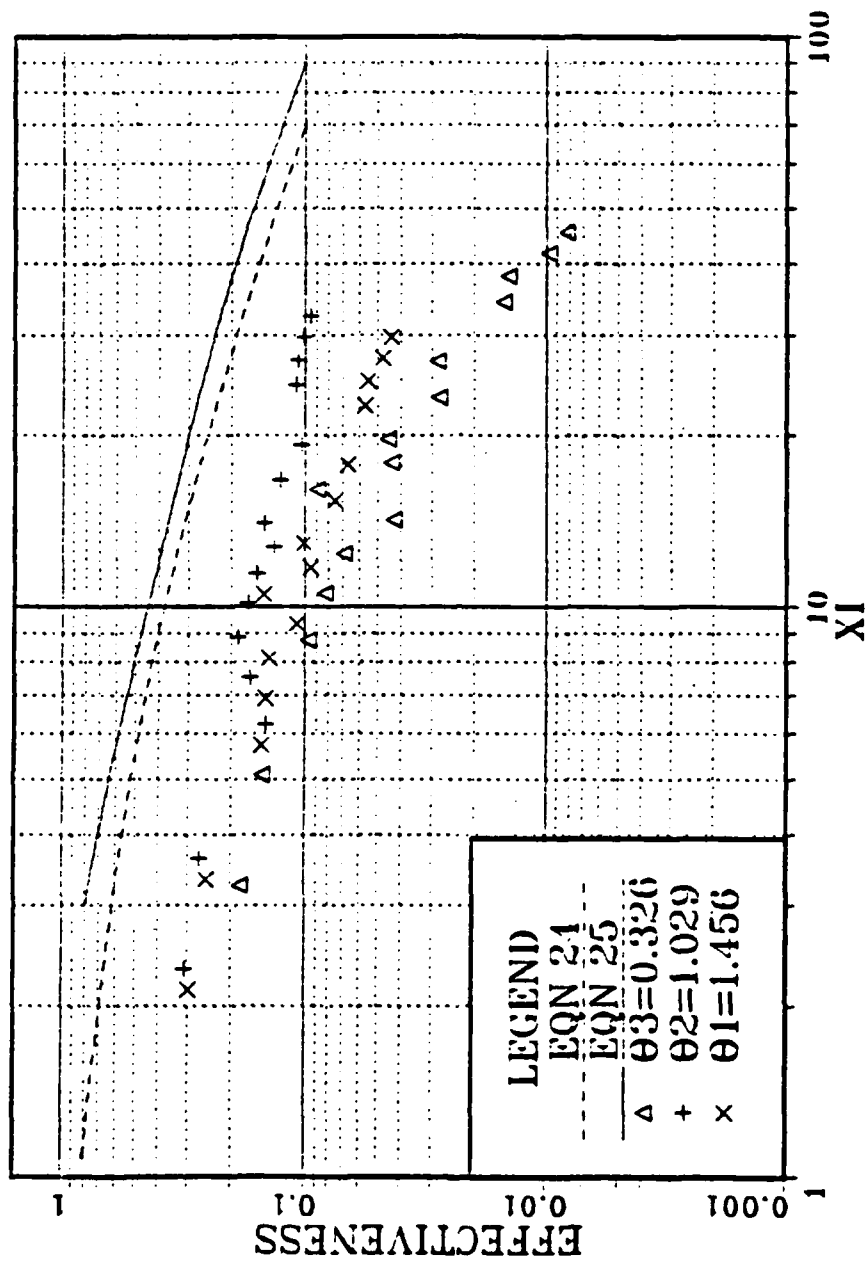


Fig. 40 Variation of  $\hat{\eta}$  with  $\xi$  for  $u_c/u_\infty = 0.630$ .

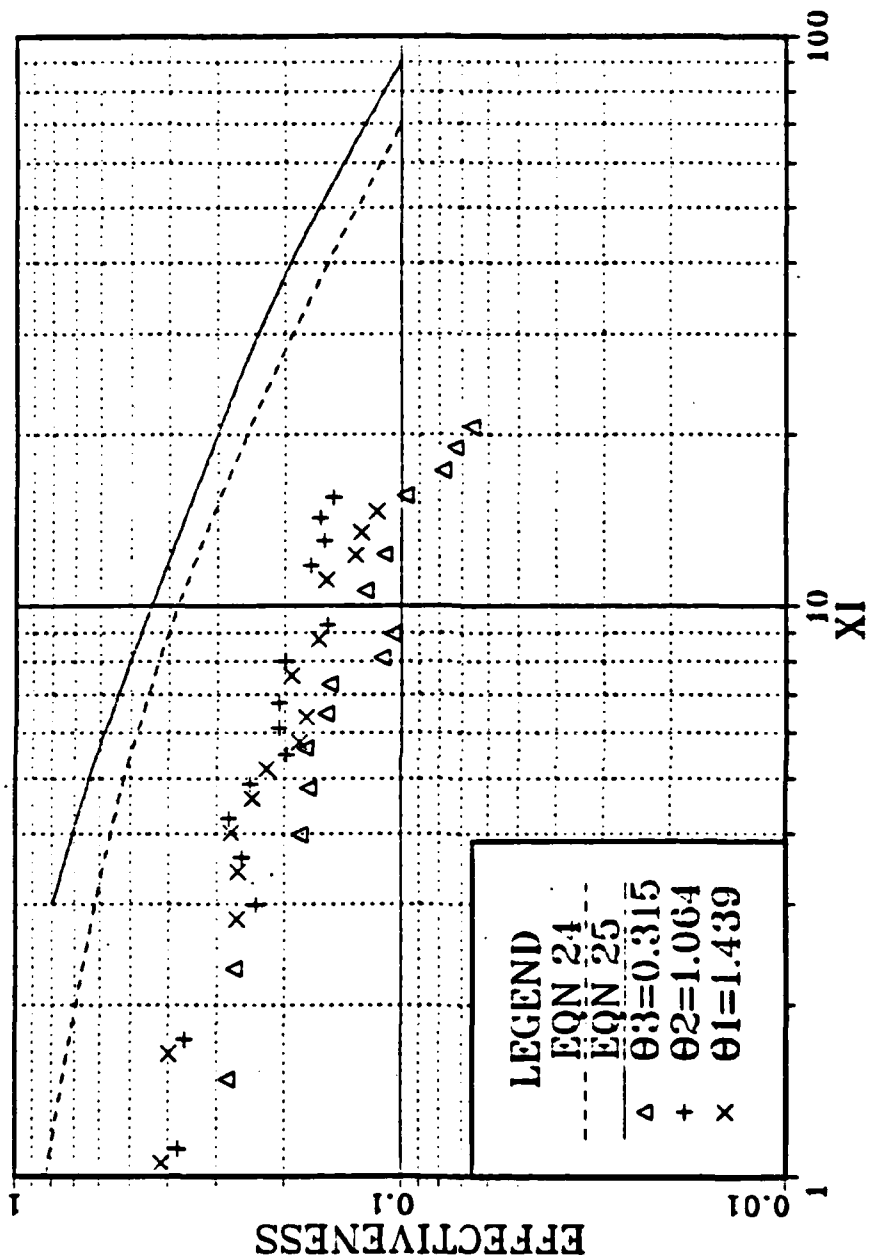


Fig. 41 Variation of  $\hat{\eta}$  with  $\xi$  for  $u_c/u_\infty = 1.113$ .

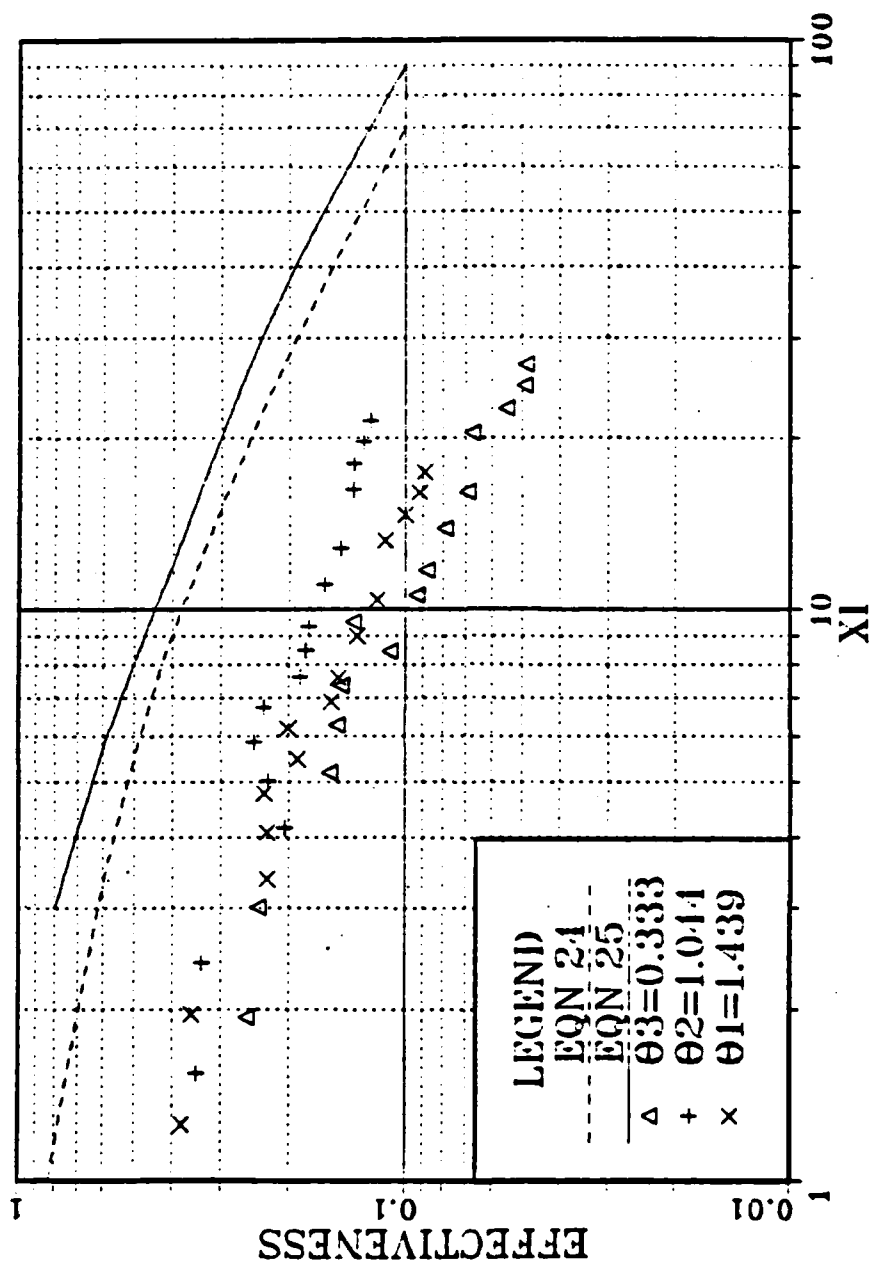


Fig. 42 Variation of  $\hat{\eta}$  with  $\xi$  for  $u_c/u_\infty = 0.922$ .

# INITIAL DISTRIBUTION LIST

	No.	Copies
1. Defense Technical Information Center Cameron Station Alexandria, Virginia 22304-6145	2	
2. Library, Code 0142 Naval Postgraduate School Monterey, California 93943-5002	2	
3. Department Chairman, Code 69 Department of Mechanical Engineering Naval Postgraduate School Monterey, California 93943	1	
4. Professor P. M. Ligrani, Code 69XK Department of Mechanical Engineering Naval Postgraduate School Monterey, California 93943	5	
5. Professor K. T. Yang, Code 69 Department of Mechanical Engineering Naval Postgraduate School Monterey, California 93943	1	
6. LCDR. A. F. Walz, USN 485 Phillip Drive Sierra Vista, Arizona 85635	1	

END

DTIC

6-86